1-1-2010

Application Of A Thermodynamic-Based Model To Investigate Bone Remodeling After Total Hip Arthroplasty Using Different Hip Implants

Alireza Sayyidmousavi
Ryerson University

APPLICATION OF A THERMODYNAMIC-BASED MODEL TO INVESTIGATE BONE REMODELING AFTER TOTAL HIP ARTHROPLASTY USING DIFFERENT HIP IMPLANTS

by

Alireza Sayyidmousavi
MASc. (Mechanical Engineering)
KN Toosi University of Technolgy (Iran), 2005

A Thesis
Presented to Ryerson University
in partial fulfilment of the
requirements for the
Degree of Master of Applied Science
in the Program of
Mechanical Engineering

Toronto, Ontario, Canada, 2010

Author's Declaration

I hereby declare that I am the sole author of this thesis.

I authorise Ryerson University to lend this thesis to other institutions of individuals for the purpose of scholarly research.

I further authorise Ryerson University to reproduce this thesis by photocopying or by other means, in total or in part, at the request of other institutions or individuals for the purpose of scholarly research.

Acknowledgements

It is with sincere gratitude that I recgonise my instructors, peers, and friends who helped me piece together this thesis study from the ground up:

My supervisor Dr. Habiba Bougherara, for her consistent guidance throughout the duration of this study. In addition to her instruction on composite laminates, I am grateful for her much-needed encouragement that helped me see this thesis through.

Dr. Ahmad Varvani for his invaluable help and support during my studies in Canada.

Dr. Greg Kawal and Ms. Leah Rogan, and the School of Graduate Studies at Ryerson University, for their assistance throughout the course of my post-graduate studies.

Last, but certainly not least, I recognise my parents, for their selfless, unconditional support in good times and bad. To you both, I will always remain indebted.

This page is intentionally left blank.

ABSTRACT

APPLICATION OF A THERMODYNAMIC-BASED MODEL TO INVESTIGATE BONE REMODELING AFTER TOTAL HIP ARTHROPLASTY USING DIFFERENT HIP IMPLANTS

Alireza Sayyidmousavi, MASc (Mechanical Engineering)

A thesis presented to Ryerson University in partial fulfillment of the requirements for the degree of Master of Applied Science in the program of Mechanical Engineering

Toronto, Ontario, Canada, 2010

A new thermodynamic-based model for bone remodeling is introduced. This model is based on chemical kinetics and irreversible thermodynamics in which bone is treated as a self-organizing system capable of exchanging matter, energy and entropy with its surroundings. Unlike the previous works in which mechanical loading is regarded as the only stimulus for bone remodeling, this model establishes a coupling between mechanical loading and the chemical reactions involved in the process of bone remodeling. This model is then incorporated to the finite element software ANSYS in the form of a macro to study bone remodeling after total hip arthroplasty with four different implants: Custom-made titanium, Composite, Exceter and Omnifit hip stems. Numerical computations of bone density distribution after total hip arthroplasty indicate that the Omnifit implant with carbon fiber polyamide12 composite results in minimum resorption in the proximal femur and consequently minimum bone loss due to stress shielding.

TABLE OF CONTENTS

LIST OF FIGURES

LIST OF TABLES

NOMENCLATURE

Latin

A	Chemical Affinity
E	Modulus of Elasticity
j	Flux
L	Phenomenological Coefficient
n	The Number of Moles
p	Mechanical Pressure
S	Entropy
T	Thermodynamic Temperature
U_a	Strain Energy Density
W	Work
w	Chemical Reaction Rate
X	Thermodynamic Force

Greek

Δ	Change in a property; usually followed by the notation of the property
ε	Strain
σ	Stress
v	Poisson's ratio
ρ	Density

CHAPTER 1

1 INTRODUCTION

Total hip arthroplasty, also called total hip replacement (THR), is an orthopedic surgical operation carried out to reform the hip joint. In total hip arthroplasty, the head and proximal neck of the femur (the bone that extends from the hip to the knee) as well as the surface layer of the socket (acetebulum) in the pelvis (the two large bones that rest on the lower limbs and support the spinal column) are surgically removed. An artificial canal is then created in the proximal medullary region of the femur and a femoral prosthesis, composed of a stem and a small diameter head is inserted into the femoral medullary canal. The socket in the pelvis is replaced with a plastic or a metal and plastic hemispherical cup. A liner that is most often made of ultra-high molecular weight polyethylene is inserted in the cup that forms the new acetabular surface that articulates with the ball on the femoral stem to minimize bone to bone friction [1]. Figure 1.1 shows a normal hip joint and a total hip arthroplasty.

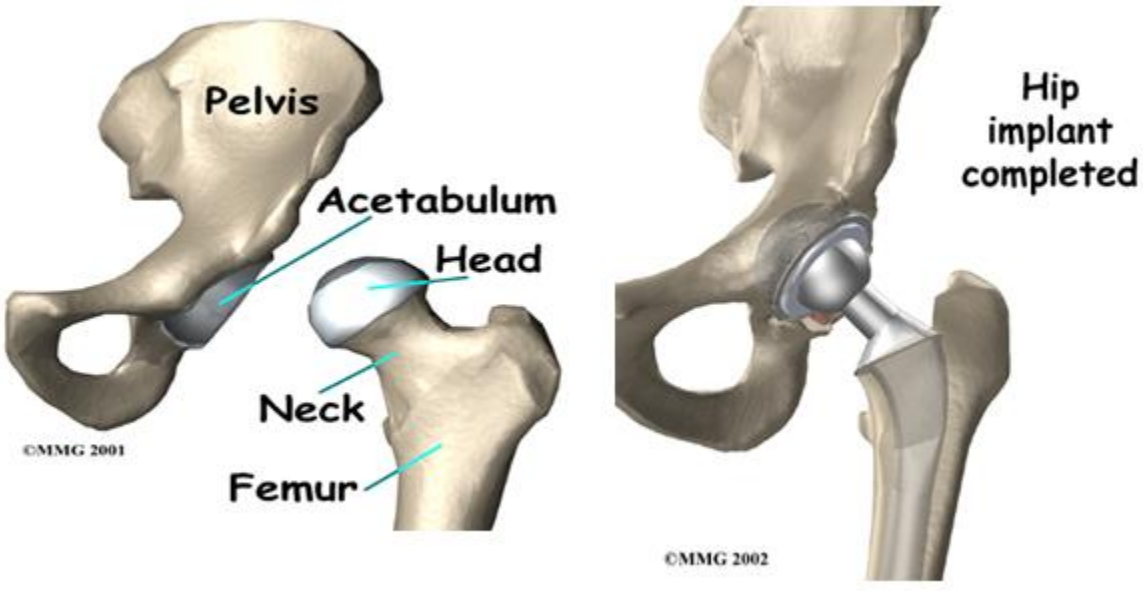

Figure 1.1: Normal Hip Joint (left), Total Hip Arthroplasty (right) [2]

Total hip artroplasty may be carried out for people suffering from a variety of hip problems either due to a disease or an injury. Some of the most common diseases which lead to total hip arthroplasty are introduced later.

One of the most important concerns following total hip arthroplasty is bone loss in the proximal part of the femur which is believed to be as a result of a phenomenon called stress shielding [3]. Based on a simple mechanical rule, if a system which is composed of two different materials is loaded, the stiffer component will sustain the greater part of the load. This is exactly what happens after hip arthroplasty. Femoral implant which has been inserted in the medullary canal of the femur is much stiffer than the natural skeleton of the body and will therefore take a greater part of the body weight load i.e. the implant is overloaded whereas the skeleton surrounding it is unloaded resulting in bone loss and decreased bone density [4]. Figure 1.2 illustrates a simple scheme of the stress shielding phenomenon.

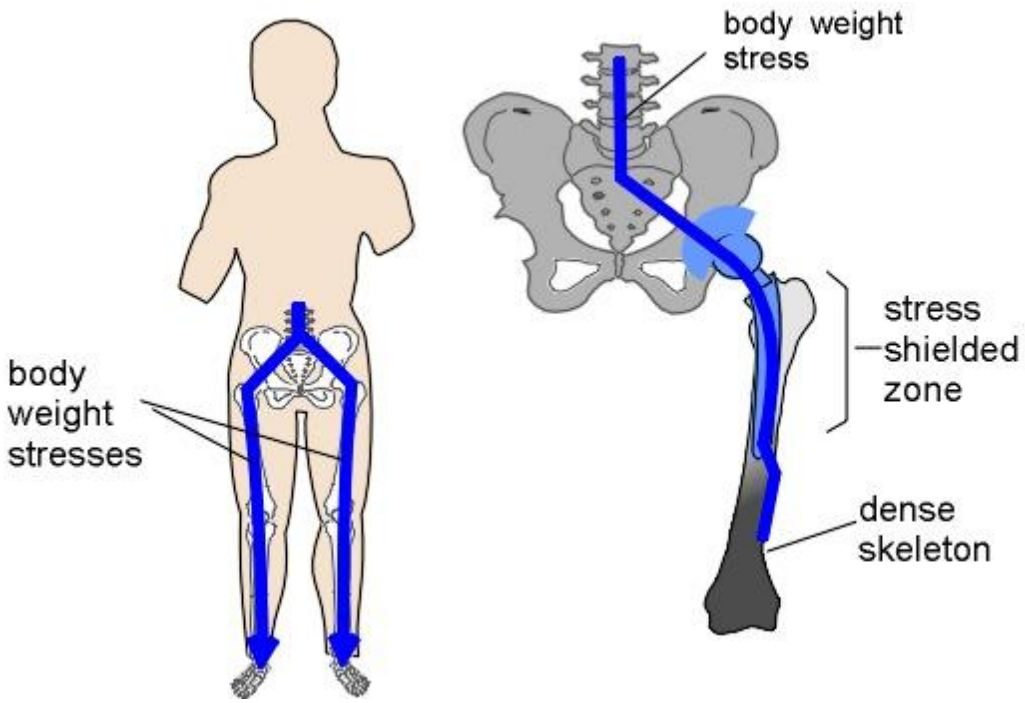

Figure 1.2: A Simple Scheme of Stress Shielding [5]

This bone loss leads to the gradual loosening of the implant which may call for a revision surgery especially for young patients due to higher loads on the prosthesis [6]. Surgical revision

is technically more difficult than the primary total hip arthroplasty procedure, both because there is less bone stock to work with and because the removal of the prosthetic components may result in fracture or perforation of the bone [1]. Although success has been continuously achieved with most of total hip arthroplasties over the past 40 years, factors related to implant longevity and a younger more active population of patients have led to an increase in the absolute number of failed THRs [7]. A recent prediction shows that the number of revision surgeries will increase 137% from 2005 to 2013 in the United States. [8]. It is therefore of great clinical importance to improve the survivability of hip implants and reduce the rate of total hip revision through predicting how bone adapts itself in response to its mechanical loading environment (bone remodeling) after total hip arthroplasty [9]. Since it is not always possible to assess bone loss around implants using clinical studies, it is important to develop models to simulate bone loss. Besides, it is not possible to use clinical techniques to observe the bone remodeling process within the femoral head or specific regions of the femoral neck following total hip arthroplasty. Clinical studies may also be difficult, expensive and time consuming. For all these reasons, a computer model which can predict bone remodeling after total hip arthroplasty with different implants is extremely useful.

The current study introduces a thermodynamics-based model for the bone remodeling process in which bone is treated as an open self-organizing system capable of exchanging matter, energy and entropy with its surroundings. This thermodynamic model is then incorporated to the finite element software ANSYS in form of a macro in ANSYS Parametric Design Language (APDL) to study bone remodeling following total hip arthroplasty with four different implants: Custom-made titanium, Composite, Stryker Exceter and Stryker Omnifit hip stems. The thermodynamic-based model for bone remodeling and its finite element implementation are explained in chapter 2. Chapter 3 outlines the geometry of the CAD models and the properties of the finite element models of the femur and the implants. Finally, the results and discussions are presented in chapter 4.

1.1 Bone Function

Bone is a tissue with many functions. Basically all bones have the mechanical function of providing structural scaffolding that allows the muscles to contract. In additions, bones have the protective function of providing a casing for the vital organs of the body e.g. skull protects the

brain, ribs protect lungs and heart and pelvis protects bladder. Bone stores 99% of the body's calcium and a good portion of other ions like sodium, magnesium and phosphate. Bone marrow in the intermedullary canal (the hollow space in the middle of long bones) is responsible for the formation and development of red blood cells which are responsible for delivering oxygen to all the cells in the body [10].

1.2 Bone Structure

Two microscopically different types of the bone are distinguished: cortical or compact bone and trabecular or cancellous bone. Cortical bone is found mainly in the central cylindrical shaft of long bones, whereas trabecular bone exists at the end of long bones and within vertebrae. Figure 1.3 shows the cortical and trabecular bone in the proximal femur.

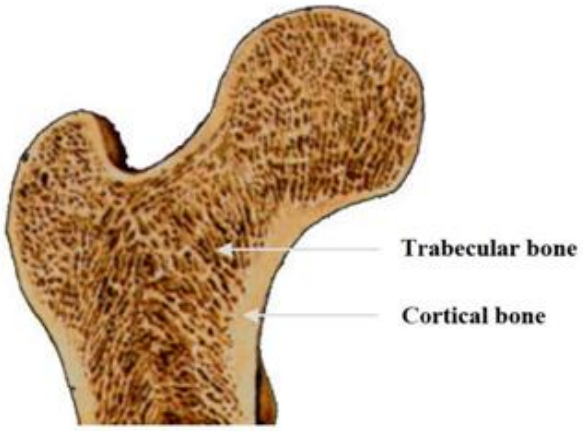

Figure 1.3: Trabecular and Cortical Bone in the Proximal Femur [11]

Cortical bone is a dense, solid tissue with a 95% volume fraction that forms the outer wall of all bones and is primarily responsible for supporting and protecting the skeleton. The tubular structure of the cortical bone provides a high moment of inertia that resists bending. At the microstructural level (100-500 microns), cortical bone has repeating structural units called osteon. An osteon is a set of concentric lamellae (thin plate structures) like the rings in a tree. Surrounding the outer border is a thin layer of mineralized matrix called cement lines. Trabecular bone is a porous cellular solid with a volume fraction of approximately 20%. It has a three

dimensional structure of interconnecting plates and rods, called trabeculae which are less than 300 μm in thickness. Figure 1.4 shows the microstructure of trabecular and cortical bone.

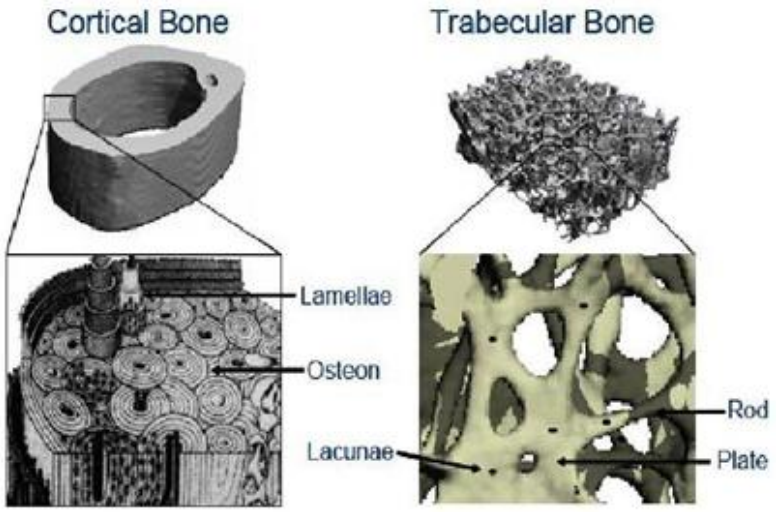

Figure 1.4: Microstructural Features of Cortical and Trabecular Bone [12]

1.3 Bone Remodeling

Bone remodeling is defined as the ability of the bone to adopt itself to the mechanical loads acting upon it by changing its size, shape and structure. In fact bone remodeling is based on Wolff's law (Wolff, 1982) according to which bone is laid down where needed and resorbed where not needed [10]. Bone remodeling is a coupled process which involves localized removal of the old bone (resorption) and replacement with newly formed bone (formation). The resorption and formation of the bone in a healthy person are in balance to maintain skeletal strength and integrity. Bone remodeling is based on the separate but coupled actions of bone resorbing cells called osteoclasts and bone forming cells called osteoblasts. Figure 1.5 illustrates the remodeling process. In the first phase called resorption (phase1), osteoclats attach to the trabecular bone surface and break down the bone by eroding the mineral and matrix. After the completion of the resorption phase, small cavities are formed on the surface of the trabecular bone (phase2). Bone forming cells (osteoblasts) start repairing the surface and filling the cavities

with the new bone which is yet to be mineralized (phase3). Finally in phase4, the bone surface is restored and covered by a layer of bone cells called lining cells. The new bone is calcified and the remodeling process is completed.

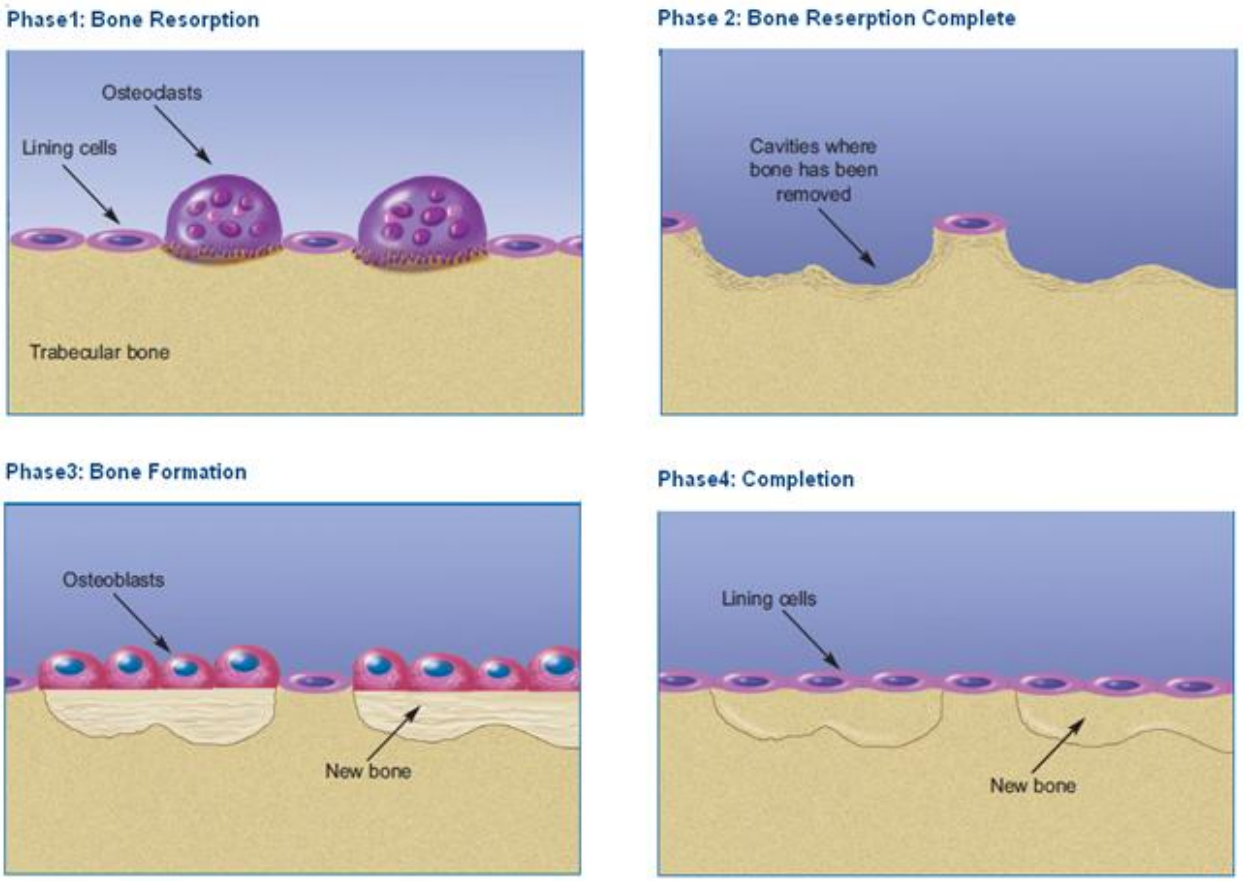

Figure 1.5: An Illustration of the Bone Remodeling Process [13]

1.4 A Literature Review on Bone Remodeling

Based on Wolff's law, it is obvious that mechanical loading has a great influence on the bone remodeling process. Several mathematical models have been proposed to explain the bone remodeling phenomenon. These models may be divided into three groups: Mechanical, mechanobiological and biochemical.

Mechanical models are based on the assumption that a mechanical signal within the bone initiates change in the shape and density of the bone without considering the underlying biological processes that induce bone remodeling. This mechanical signal can be stress, strain,

strain energy density or mechanical damage [14-16]. The strain energy based model is probably the most popular model which is based on Frost's mechanostat theory. This theory states that there is a minimum effective strain which must be exceeded to excite an adaptive response to mechanical over load. It suggests that there is a range of strain values (known as the dead zone) that will cause no response. Strain above this range will cause bone formation and strain below this range will initiate bone resorption [17]. Weinans et al. [14] formulated this concept and used the strain energy density as the stimulus that evokes bone remodeling.

$$\frac{d\rho}{dt} = B(\frac{U_a}{\rho} - K)$$ **Equation 1.1**

Where $U_a = \frac{1}{n}\sum_{i=1}^{n} U_i$; U_i is the apparent energy density (*SED*) for the load casing *i* and *n* is the number of loading cases during the gait cycle. *B* and *K* are the scaling factor and a reference value, respectively.

Another example of such models is the one developed by Levenston and Carter [16] which proposes a model for bone adaptation based on cyclic energy dissipation as a measure of bone damage. According to this model, when damage is created during cyclic loading of the bone, a portion of the energy transferred during the loading phase is not recovered during the unloading phase. This energy is dissipated through some damage process such as the creation and extension of fracture surfaces. Therefore, the energy dissipated in a loading cycle can be used as a measure of the damage created during that cycle. In this model, the stimulus which initiates bone remodeling is formulated as proportional to the damage energy dissipation summed over all daily loading cycles.

$$S \propto \sum_{k=1}^{N} H_{Dk}$$ **Equation 1.2**

Where *N* is the number of loading cycles in a given day and H_{DK} is the density of the dissipated energy for the K^{th} loading cycle which can be measured experimentally as the hysteresis on a stress-strain curve. Although these models have been to some extent successful in predicting normal bone architecture, they suffer from three major drawbacks [15]. First they use only mechanical signals to simulate bone remodeling and fail to consider the underlying biological mechanisms. Second, they consider bone as a continuum material and thus apply theories of

linear elasticity. Third, the theories behind most of these models are quasi static and do not include the effects of load rates and nonlinear (viscoelastic) properties.

Mechanobiological models aim at taking into effect biological as well as mechanical factors of bone remodeling. Several mechanobilogical models have so far been presented [18-20]. A mechanobiological model, developed by Huiskes et.al, [18] is based upon the separation of osteoblastic and osteoclastic activities. According to this model, osteoclasts are recruited and activated either where microcracks occur or in disused areas in the bone. The dynamic forces of daily living are known to produce microcracks. It is likely that these microcracks can occur anywhere, at any time for a normally functioning individual, in other words, the distribution of these microcracks is random. Mechanosensitive cells, called osteocytes, which derive from osteoblasts, sense a mechanical signal due to external load transfer through the architecture and locally recruit osteoblast to do the bone formation. The mechanical signal which is sensed by osteocytes is assumed to be the strain energy density. This process is illustrated in Figure 1.6.

Biochemical models are based on the activities of osteoblasts and osteoclasts to obtain an insight into the bone remodeling process at a cellular level [21]. The first model of this kind described the differential activity of the Parathyroid Hormone (PTH) which acts as a regulator for bone resorption and formation [22, 23]. Another biochemical model, developed by Komarova et.al, [24], studied the role of hormones such as autocrine and paractine in the regulation of bone remodeling. A recent model of this kind proposed a signaling pathway known as RANK/RANKL/OPG to regulate bone cell activities [25]. The most noticeable defect of these cell-based models is that they do not consider the mechanical stimulus of the bone remodeling process. However, a good model should take into account all different factors that are involved in bone remodeling process. The current study introduces a thermodynamics-based model for the bone remodeling process aims at taking mechanical, chemical, biological factors into consideration. This model treats bone as an open self-organizing system capable of exchanging matter, energy and entropy with its surroundings. This thermodynamic model is then incorporated to the finite element software ANSYS in form of a macro in ANSYS Parametric Design Language (APDL) to study bone remodeling following total hip arthroplasty with four different implants: Custom-made titanium, Composite, Stryker Exceter and Stryker Omnifit hip stems.

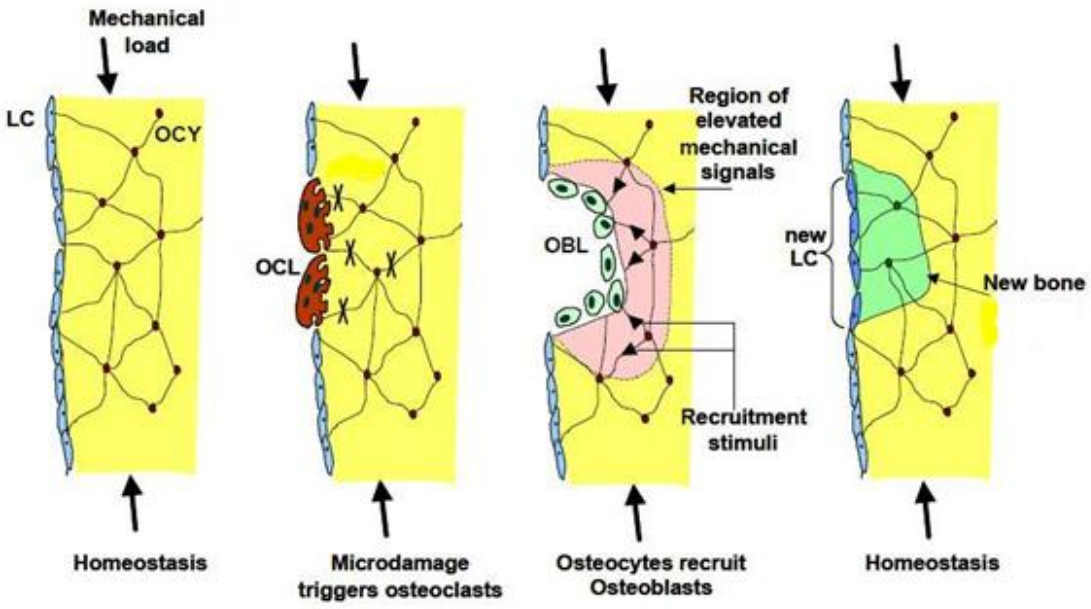

Figure 1.6: The Remodeling Process Based on Hueskis Model [18]

1.5 Strain Energy Density Model

Since the strain energy density is regarded as the mechanical stimulus in most of models for the bone remodeling process and in order to compare it with the novel thermodynamic based model presented in chapter 5, it seems worthy to explain this model in more detail.

The mechanical variable in this model is the strain energy which can be expressed by the stresses and strains as:

$$U = \frac{1}{2}\{\sigma\}\{\varepsilon\}$$ **Equation 1.3**

Based on these variables, a stimulus is determined which controls the rate of remodeling. Then relation between the strain energy and the change of the bone density with time defines the remodeling governing rule. The actual bone density is related to the modulus of elasticity of the bone which is fed into the Finite Element model as an input. This iterative process stops when no significant changes in the density of the elements are observed. The remodeling governing equation is stated as:

$$\frac{d\rho}{dt} = B\left(\frac{U_a}{\rho} - k(1+s)\right) \qquad \frac{U_a}{\rho} \geq k(1+s)$$ **Equation 1.4a**

$$\frac{d\rho}{dt} = B\left(\frac{U_a}{\rho} - k(1-s)\right) \qquad \frac{U_a}{\rho} \le k(1-s)$$ **Equation 1.4b**

$$\frac{d\rho}{dt} = 0 \qquad k(1-s) < \frac{U_a}{\rho} < k(1+s)$$ **Equation 1.4c**

The occurrence of bone resorption or formation depends on the value of the quantity U_a/ρ, when the value of $U_a/\rho - k \neq 0$, the drive force which causes formation and resorption does exist. If this driving force is positive, bone formation is induced. If the driving force is negative, bone resorption will take place. However, in practice, there are certain values of this driving force which causes neither resorption nor formation. This range of values which is denoted by s referred to as the dead zone. The boundary condition for the predicted density is expressed as:

$$\rho_{\min} \le \rho \le \rho_{\max}$$ **Equation 1.5**

The relation between the elastic modulus and the bone density is taken as:

$$E = C\rho^D$$ **Equation 1.6**

The constants C and D are determined by homogenization method [9]. Figure 1.7 shows a visualization of Equation 1.4.

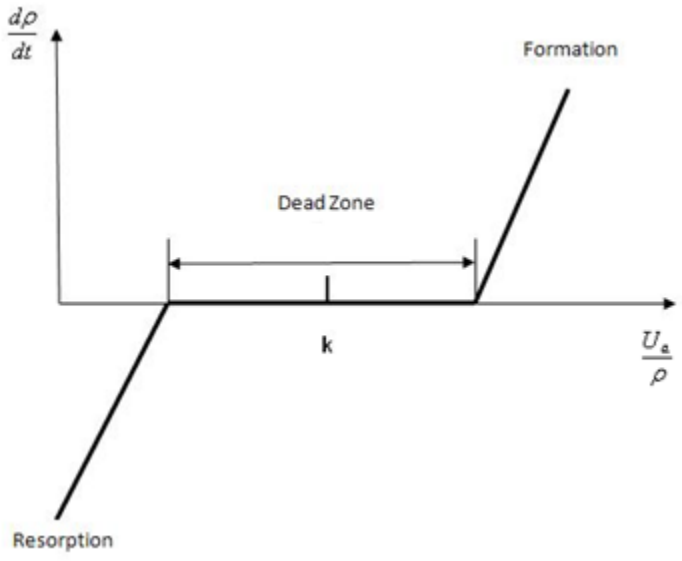

Figure 1.7: Bone Remodeling as Described by Frost

1.6 Hip Joint

Hip joint is a ball-socket joint which is composed of the acetabulum and femur (Figure 1.8). It allows for a wide range of motions necessary for normal daily activities such as walking, sitting and squatting.

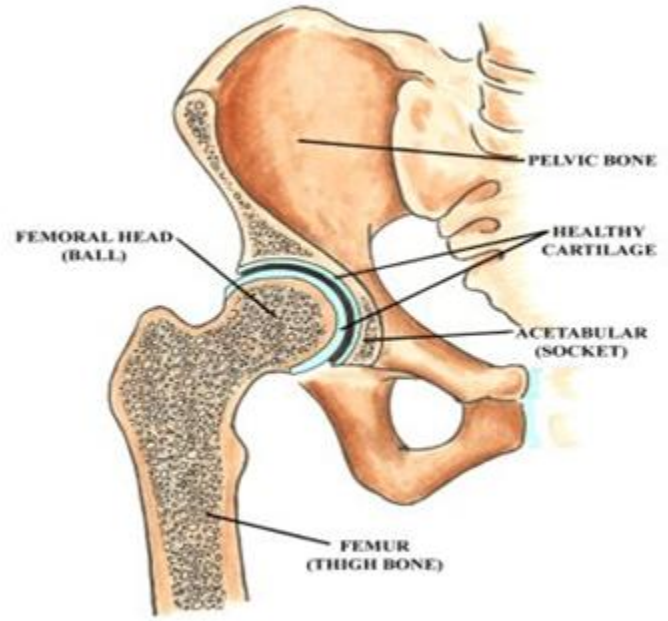

Figure 1.8: Different Components of A Healthy Hip Joint [26]

1.7 The Acetabulum

The acetabulum is the socket component of the hip joint into which the femoral head fits. The acetebular surface is covered with a cartilage which thickens peripherally. This cartilage is to minimize friction between the acetabulum and the femur head. The cavity of the acetabulum faces obliquely forward, outward and downward [10].

1.8 The Femur

The femur, which is also known as the thighbone, is the longest, heaviest and strongest bone in human body that extends from hip to knee. It is connected to the acetabulum at the proximal end and to the knee at the distal end. The average human femur is 48 centimetres in length and 2.34 centimetres in diameter and can support up to 30 times the weight of an adult. The proximal end consists of the femoral neck and the femoral head. The neck of the femur is a flattened bone

which connects the femoral head to the femoral shaft. The femoral head is the highest part of the femur and fits into the acetabulum. It is globular and forms rather more than a hemisphere [27]. The neck and head of the femur are mainly composed of trabecular bone whereas the femoral shaft is primarily made up of cortical bone.

1.9 The Gait Cycle

Before studying the mechanical loads exerted on the hip joint. Since walking is the most common and important activity which induces cyclic load on the hip joint, it is useful to become familiar with the gait cycle which describes the simple activity of walking. Figure 1.9 demonstrates the human gait cycle.

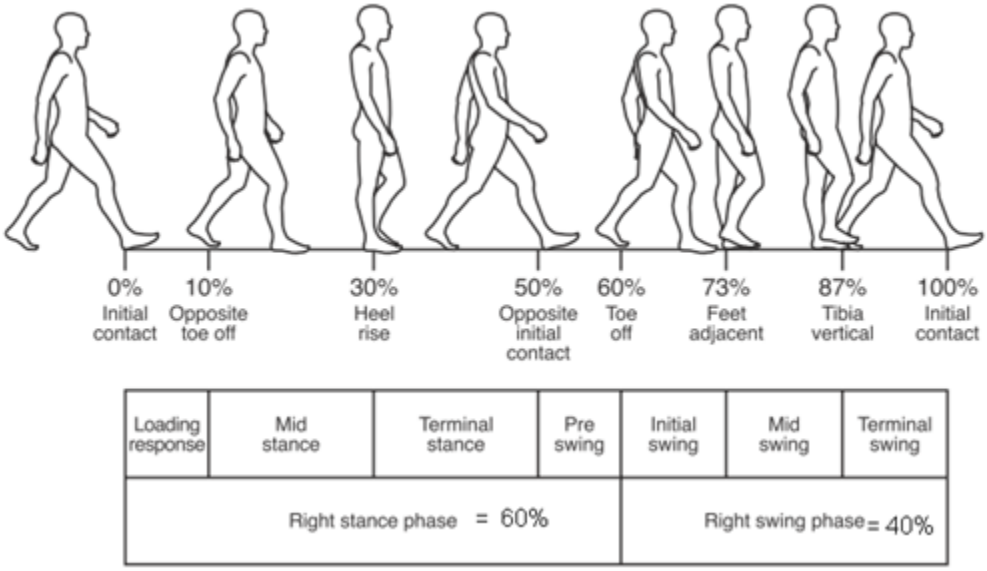

Figure 1.9: The Human Gait Cycle [27]

As can be seen in the Figure, one gait cycle is understood to begin when one foot contacts the ground until the same foot contacts the ground again. It is estimated that an average adult takes around 1-1.5 million steps annually [28]. There are two primary phases of gait, the stance phase and the swing phase. Stance phase is 60% of the gait and the swing phase is 40% approximately. The loading response, mid-stance, terminal stance, and the pre-swing are the further divisions of the stance phase. The moment at which the foot comes into contact with the ground is the beginning of the loading response. It ends when the toes of the opposite leg leave the ground. Mid-stance begins at the contralateral toe-off, and ends when the body centre of gravity is

directly over the reference foot. At this moment, the terminal stance starts and ends when the foot of the other leg contacts the ground. At the contralateral initial contact, the pre-swing begins and ends when the toes of the reference leg leave the ground. The initial swing, mid-swing, and the terminal swing are the further divisions of the swing phase. The initial swing stage starts at toe-off, and continues until the reference knee reaches a maximum flexion of around 60 degrees. Mid-swing starts and ends from the maximum knee flexion to until the knee is perpendicular to the ground. Terminal swing starts when the knee is perpendicular to the ground and ends at initial contact and then the gait cycle starts over again [29].

1.10 The Structural Loads on the Hip Joint

Ultimate load transfer and stability are two major factors which need to be taken into account for a proper design of an implant which is to minimize stress shielding. To that aim, a basic knowledge of the force system acting on the hip joint is vital.

- **Static Loading**

Figure 1.10 shows the external forces acting on the body during a single-leg stance equilibrium position. The reaction force from the ground is equal to the body weight w. The gravitational force of the stance leg is *W/6* [10]. Therefore, the remaining force will be *5W/6*.

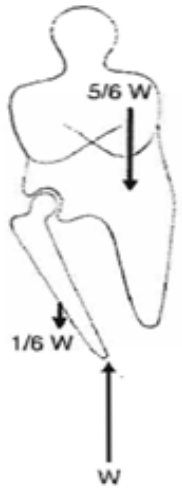

Figure 1.10: The External Forces on the Body in a Single-Leg Stance Equilibrium Position [10]

To find the internal forces acting on the hip joint, the hip joint is divided to an upper and a lower free body as shown Figure 1.11. For the upper free body, the equilibrium is obtained if

the moment of the force of the abductor muscle *M* about the centre of rotation of femoral head (point Q) counterbalances the moment caused by the gravitational force of the superincumbent body.

$$\frac{5W}{6} \times b - (M \times c) = 0 \Rightarrow M = \frac{5W \times b}{6c}$$ **Equation 1.7**

Where b is the gravitational force lever arm and c is the abductor force lever arm .The direction of the muscle force can be estimated from the muscle origin and insertion on roentgenogram so that the values of M_x and M_y are estimated to be *W* and *1.7W*, respectively [10]. Turning now to the lower free body the components of the joint force can be determined by writing the equilibrium equations in horizontal and vertical directions.

$$\sum F_x = 0 \Rightarrow J_x = M_x = W$$ **Equation 1.8**

$$\sum F_y = 0 \Rightarrow J_y = W + M_y - \frac{W}{6} = 2.5W$$

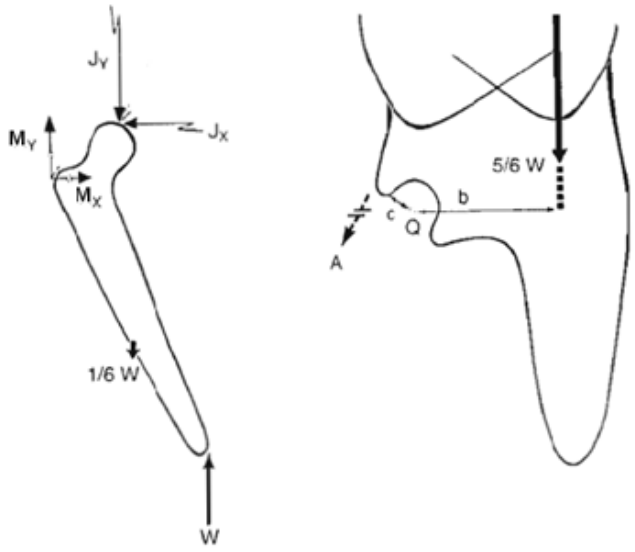

Figure 1.11: The Internal Forces on the Hip Joint in a Single-Leg Stance Equilibrium Position [10]

- **Dynamic Loading**

The loads on the hip joint during dynamic activities have been studied by several researchers. Paul (1967) studied the joint reaction force on the femoral head in normal men and women during gate and correlated the peak magnitudes with specific muscle activity recorded electromyographically [10]. As Figure 1.12 shows, in men two peak forces were observed during the stance phase. One peak about four times body weight just after heel strike and another one about seven times the body weight, just before toe off. During foot flat, since the centre of gravity of the body continues to lower, the joint reaction force decreases to a values less than the body weight. During the swing phase, the magnitude of the joint force remains equal to the body weight. Although the force pattern was almost the same for women, the magnitude was to some extent lower with a maximum of only four times the body weight. This can be attributed to several factors: a wider female pelvis, a difference in the inclination of the femoral neck-shaft angle, a difference in foot wear and differences in the general pattern of gait [10].

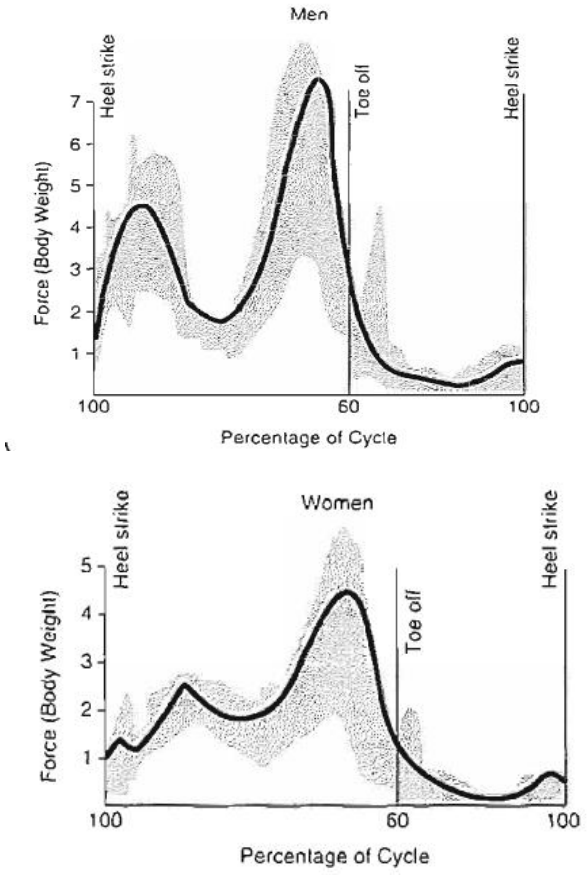

Figure 1.12: Hip Joint Reaction Force During One Gait Cycle [10]

1.11 A History of Total Hip Arthroplasty

Identifying the physiology of the skeletal tissues during the first half of the eighteenth century expedited the progress in the field of operative orthopedics by the end of that century. Anthony White (1782-1849) of the Westminster hospital in London is believed the first surgeon to have performed modern excision arthroplasty in 1821 although he did not make a personal report of the operation [30]. However, John Rhea Barton (1794-1871) in Philadelphia is credited with performing the first osteotomy on a diseased hip in 1826. During the 1830s -1880s, attempts were made to restore mobility by using interpositional membranes between the femoral head and acetabulum in which materials such as wooden blocks and animal soft tissues were tried. The first prosthetic hip replacement was carried out by a German Professor called Themistocles Gluck who produced an ivory ball and socket joint that were fixed to the bone with nickel-plated screws. He also used a mixture of plaster of Paris and powdered pumis with resin to provide fixation. At the turn of the eighteenth century John Benjamin Murphy (1857-1916) adopted a more reasonable approach in which he just removed the overhanging bone osteophytes from the base of the femur head and the rim of the acetabulum. A French surgeon called Foedre introduced pig bladder as the interpositional material which was strong enough to withstand the stresses of weight bearing and intra-articular pressure. At the same time, Sir Robert Jones (1855-1933) used a strip of gold foil to cover reconstructed femoral head. After twenty-one years, the joint was still effective which to that point, was the longest living joint [31]. In 1924, the procedure for osteoarthritis surgery by means other than fusion was described for the first time by Royal Whitman (1857-1946). In the operation, the head of the femur was removed and trochanter was cut from the shaft in an oblique direction with all its attached muscles so that the additional area together with the part of the neck that remained provided a secure weight. Though this procedure was further modified by several researchers, no actual success was achieved. In fact in order to relieve pain, either mobility or stability had to be sacrificed. In 1923, Marius Smith Peterson, an American surgeon, performed interpositional arthroplasty with a mould prosthesis which was aimed at facilitating bone the movement of the bone implant at both the femoral and acetabular sides. Having seen a smooth membrane around an excised piece of glass, he decided to design a glass mould to be placed between the femoral head and the acetabulum. This type of mould, according to Peterson, would “guide nature’s repair”. However some of the moulds broke and although he was optimistic about the success of this type mould,

the stubbornness of his patients who persisted in their ailments made him abandon the idea. In 1937, following a suggestion put forward by his dentist, he designed vitallium moulds which yielded satisfactory clinical results within the following ten years. In fact, this type of mould provided the first predictable result in interdispositional arthroplasty.

Pier Delbet (1826-1925) was the first to use a rubber femoral prosthesis to replace one half of the hip joint. In 1927, Ernest W. Heygroves (1872-1944) used ivory. In 1948, Judet brothers, Robert (1901-80) and Jean (1905-95) from Paris, France used an acrylic prosthesis which failed pretty soon because of being extremely vulnerable to wear . In 1950, Fredrick Roeck Thomson (1907-83) refined the Judet brothers' idea by developing Vittalium prosthesis. Austin Moore (1899-1963) and Harold R. Bohlman modified this prosthesis by placing a flared collar below the head and a vertical intermedullary stem. Moore inserted this prosthesis at John Hopkins Hospital in 1940 in an operation where he replaced twelve inches of a femur with a custom made Vitallium prosthesis. Moore and Bohlman refined this implant further. The new implant featured a fenestrated stem which allowed bone ingrowth. These two implants were the first hip arthroplasty products that were distributed in large numbers and are still used for the replacement of the femoral head and neck [30].

The first total hip replacement is believed to have been carried out by Philip Wiles in 1938 [1] using accurately fitted stainless steel components which were fixed to the bone with screws and bolts. The procedure was further developed by Mckee and Farrar in the 1950's. These early attempts laid the foundation for Sir John Charnley who in the 1960's created low-friction arthroplasty which is regarded by many as the current standard of total hip replacement. Charnley's arthroplasty utilizes a 22 millimeter diameter femoral head with a high density polyethylene acetabular component in order to reduce friction. These prosthetic components are then fixed to the bone with polymethylmethacrylate cement.

1.12 Hip Joint Diseases

The femur as previously mentioned can support up to 30 times the weight of an adult. This makes the hip joint the largest weight-bearing joint in the body. That is why it is prone to a variety of diseases which can cause dysfunction and pain. Many of such diseases can be treated

surgically by total hip arthroplasty [32]. Some of the most common diseases of the hip joint are listed below.

- **Osteoarthritis**

Osteoarthritis is the most common form of arthritis. It is a degenerative process that deteriorates the joint at a rapid pace by breaking down the cartilage. Osteoarthritis mostly affects people in their 60s or 70's (Figure 1.13). This disease occurs mostly due to aging. With aging, the water content of the cartilage increases, and the protein makeup of the cartilage degenerates which in advanced cases lead to the total loss of the cartilage between the bones of the joints. The loss of cartilage causes friction between the bones thus resulting in pain and limitation of joint mobility.

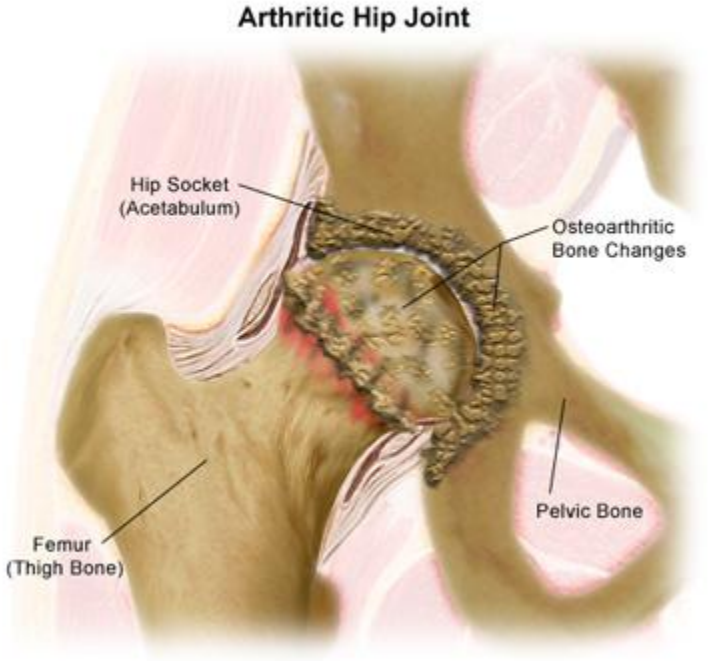

Figure 1.13: Arthritic Hip Joint [33]

- **Rheumatoid Arthritis**

Rheumatoid Arthritis is a syndrome in which the immune system attacks the tissues by mistake. If this happens to the tissues of the joint, it can cause chronic inflammation of the joint (Figure 1.14). This chronic inflammation of the joint may lead to the destruction of the cartilage at the

joint, bone and ligaments that can cause the deformity of the joint. Damage to the joints in this disease can occur early in the disease and be progressive.

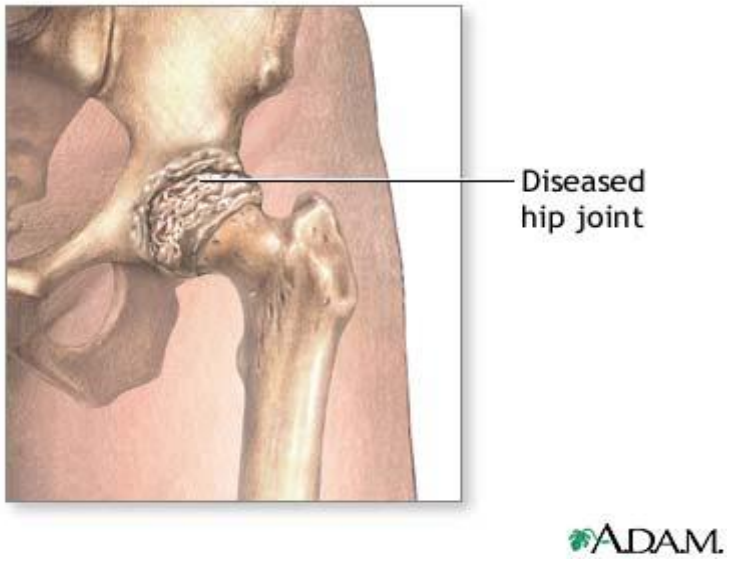

Figure 1.14: A Diseased Hip Joint Affected by Rheumatoid Arthritis [34]

- **Avascular Necrosis**

Avascular Necrosis occurs when the blood supply to the femoral head is interrupted which leads to gradual bone death and in some severe cases to the total collapse of the femoral head. Figure 1.15 shows a hip joint suffering from avescular necrosis.

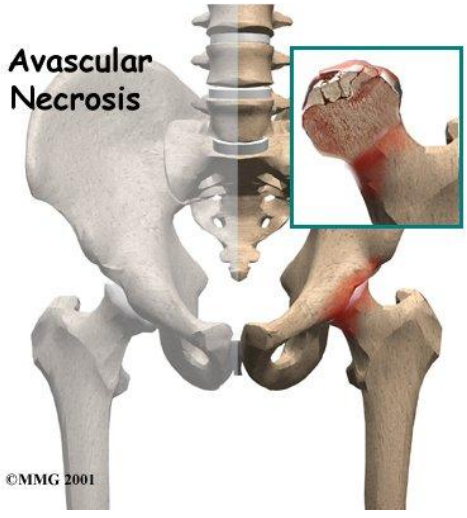

Figure 1.15: A Hip Joint Suffering from Avescular Necrosis [35]

- **Slipped Capital Femoral Epiphysis**

Slipped Capital Femoral Epiphysis (SCFE) is a disorder happening mostly in children. In SCFE, the femoral head slips off the neck of the femur. It has three degrees of severity:

- Mild: When one- third of the femoral head slips off the femur (Position A in Figure 1.16).
- Moderate: When one-third to one-half of the femoral head slips off the femur (Position B in Figure 1.16).
- Severe: When more than half of the head slips off the neck. (Position C in Figure 1.16).

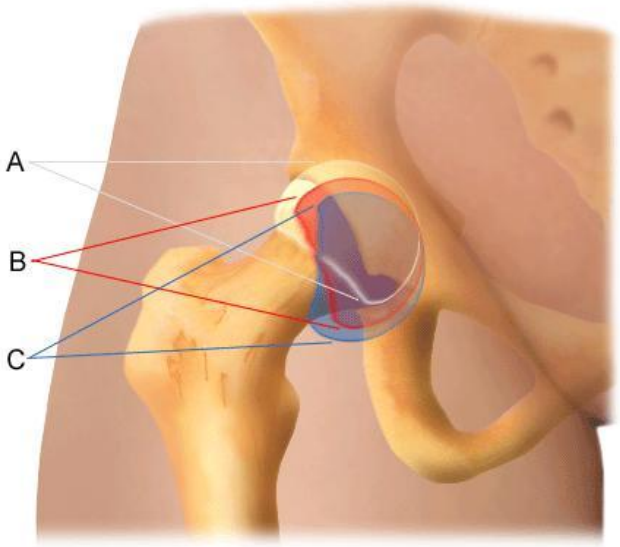

Figure 1.16: Slipped Capital Femoral Epiphysis [36]

- **Trauma**

Trauma in clues any damage to the hip joint which can be due to a fall, car accident, workplace or athletic injuries which may cause damage to the cartilage or other parts of the joint.

1.13 Total Hip Arthroplasty Procedure

In total hip arthroplasty, the damaged hip joint is replaced with a prosthesis which is implanted in the body. A total hip prosthesis has three parts (Figure 1.17).

- A plastic cup to replace the acetabulum.
- A metal ball to replace the femoral head.

- A metal stem which is attached to the shaft of the bone.

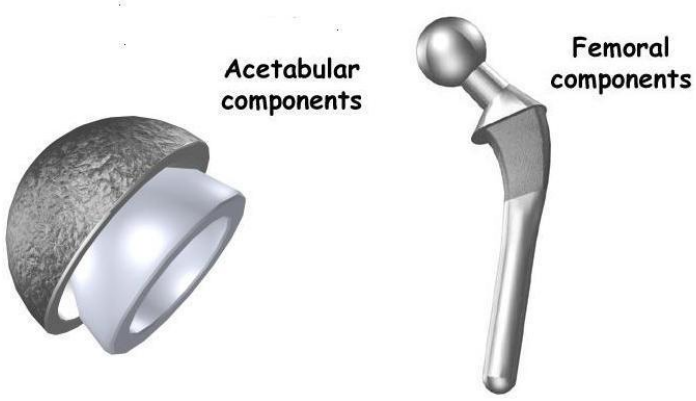

Figure 1.17: The Components of a Hip Joint Prosthesis [37]

Total hip arthroplasty is carried out for two main purposes: Pain relief and improved functioning of the joint. Figure 1.18 illustrates total hip arthroplasty procedure. A standard hip replacement operation takes 1-1/2–3 hours. After the patient is anesthetized, the surgeon makes an incision 8–12 in long down the side of the patient's upper thigh. The surgeon may then choose to enter the joint itself from the side, back, or front. The back approach is the most common. The ligaments and muscles under the skin are then separated. Once inside the joint, the surgeon separates the head of the femur from the acetabulum and removes the head with a saw. The surgeon uses a power drill and a special reamer to remove the cartilage from the acetabulum and shape it to accept the acetabular part of the prosthesis. This part of the new prosthesis is a curved piece of metal lined with plastic or ceramic. After selecting the correct size for the patient, the surgeon inserts the acetabular component. If the new joint is to be cemented, the surgeon will attach the component to the bone with a type of epoxy. Otherwise the metal plate will be held in place by screws or by the tightness of the fit itself. To replace the femoral head, the surgeon first drills a hollow inside the thighbone to accept a stem for the femoral component. The stem may be cemented in place or held in place by the tightness of the fit. A metal or ceramic ball to replace the head of the femur is then attached to the stem. After the prosthesis is in place, an x ray is taken to verify that it is correctly positioned. The staples are removed 10–14 days after surgery. Finally, a large triangular pillow known as a Charnley pillow is placed between the patient's ankles to prevent dislocation of the hip during the first few days after surgery. Another recently

introduced technique for hip replacement is called the minimally invasive surgery (MIS) where instead of making a long incision; the surgeon makes either two 2 inch incisions or one 3.5 inch incision. Using smaller tools, the surgeon then removes the damaged bone and inserts the prosthesis components. However; obese patients and those with weak bones are not recommended for this type of surgery [37].

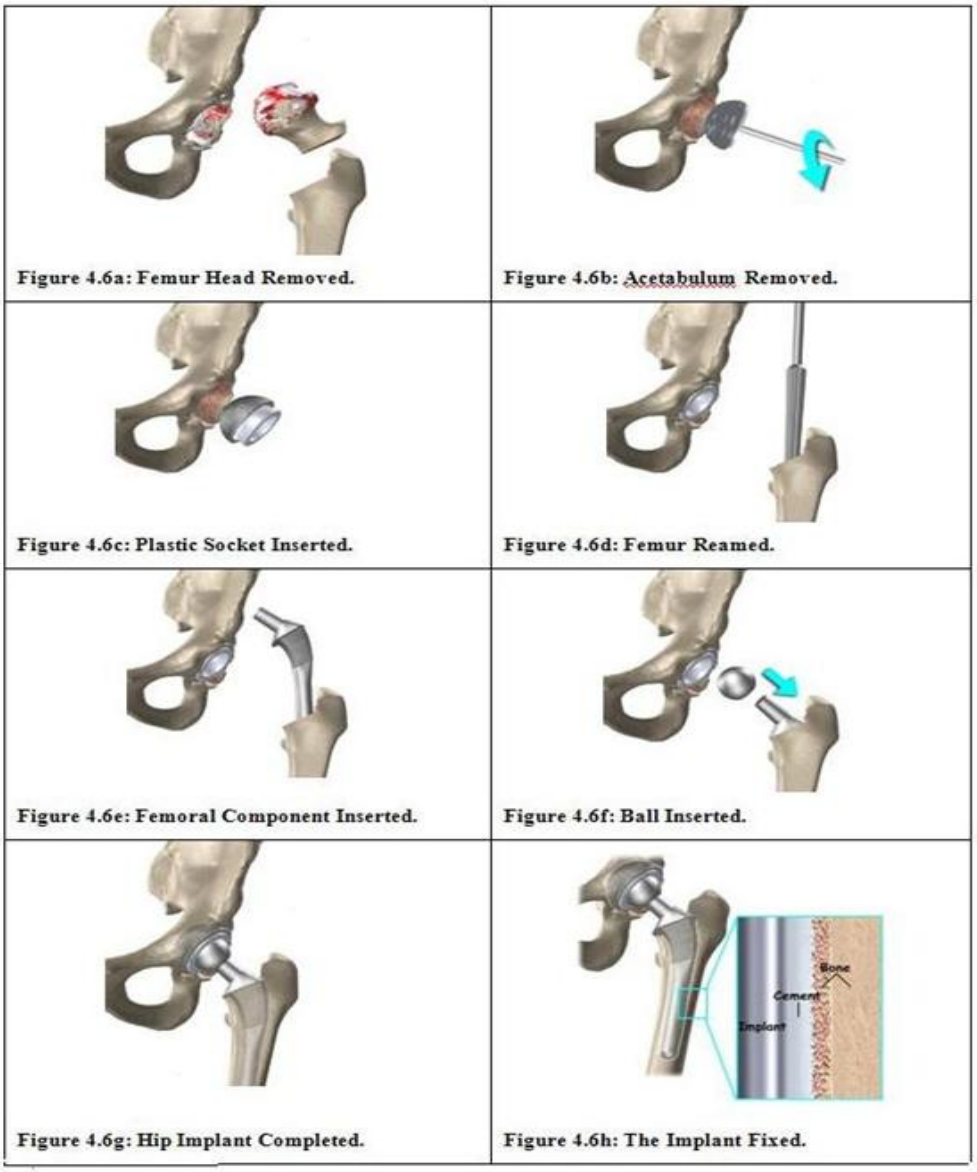

Figure 1.18: Total Hip Arthroplasty Procedure [37]

1.14 Fixation

In order to yield successful results, the components of the total hip arthroplasty must be fixed to the bone. There are mainly two methods of fixation, cemented and noncemented [1].

- **Cemented Fixation**

In this method, the implant components are fixed to the bone by means of polymethylmethacrylate cement which is a self-curing polymer without any adhesive properties. Adhesion or fixation of this polymer is achieved through two processes which are called microlocking and macrolocking. In microlocking, the cement squeezes into the small gaps and cracks of the cancellous bone. During macro buckling, the cement is fixed by filling large irregular spaces within the bone around the implant.

- **Noncemented Fixation**

Since cement debris can be problematic because of causing implant loosening, prosthesis devices have been designed to ensure fixation without using any external materials. This can be achieved by either press-fit or biological ingrowth. In the press-fit technique, by interference of the implant to the femur, whereas in biological ingrowth, fixation is achieved through the growth of bone into a porous surface which covers the implant. One method of producing porous ingrowth surface for instance in cobalt chrome prosthesis, is to fuse metal beads 250 to 400 μm in diameter into the surface of the implant. Studies have shown that ingrowth into porous surfaces start within the first 6 to 12 weeks after the surgery.

1.15 Total Hip Arthroplasty in Canada

The Canadian Joint Replacement Registry (CJRR) is a pan-Canadian organization responsible for collecting and analyzing data on hip and knee replacement operations over time. CJRR was developed through a joint effort between the Canadian Institute for Health Information (CIHI) and the orthopedic surgeons in Canada. Overview of Hip Replacement in Canada In 2006-2007, there were 24253 hospitalizations for hip replacement in Canada excluding Quebec which shows a 2.5% increase compared to 2005-2006 and a ten year increase of 37% from 15214 in 1996-1997 (Figure 1.19).

1.16 Age-Standardized Hospitalization Rates for Hip Replacement in Canada

The age-standardized hospitalization rate for hip replacement in Canada was 81.2%. This shows an increase of 25.35% compared to 1996-1997 (Figure 1.20). It is also observed that the age-standardized hospitalization rates for female were consistently higher than male during the ten year period. For males, the increase over the 10-year period was 26% (from 60.0 to 75.6), whereas for females, the 10-year increase was 24.4% (from 68.7 to 85.5).

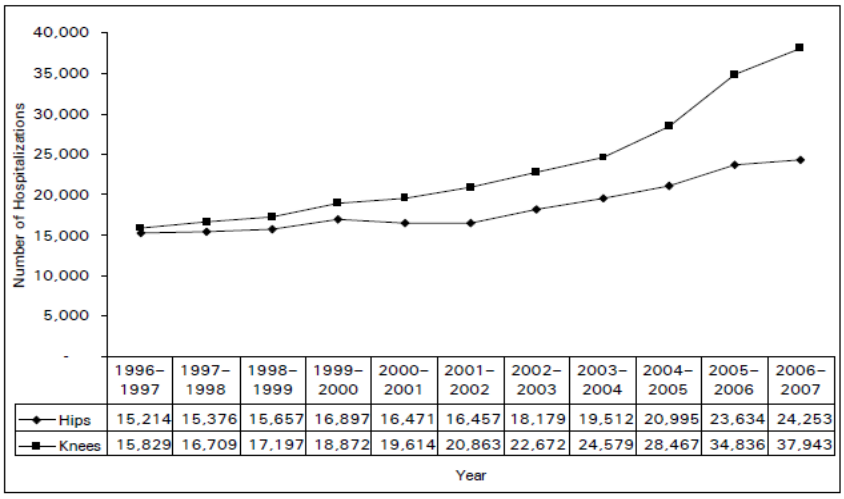

	1996–1997	1997–1998	1998–1999	1999–2000	2000–2001	2001–2002	2002–2003	2003–2004	2004–2005	2005–2006	2006–2007
Hips	15,214	15,376	15,657	16,897	16,471	16,457	18,179	19,512	20,995	23,634	24,253
Knees	15,829	16,709	17,197	18,872	19,614	20,863	22,672	24,579	28,467	34,836	37,943

Figure 1.19: Number of Hospitalizations for Hip and Knee Replacement Procedures in Canada, 1996–1997 to 2006–2007 [38]

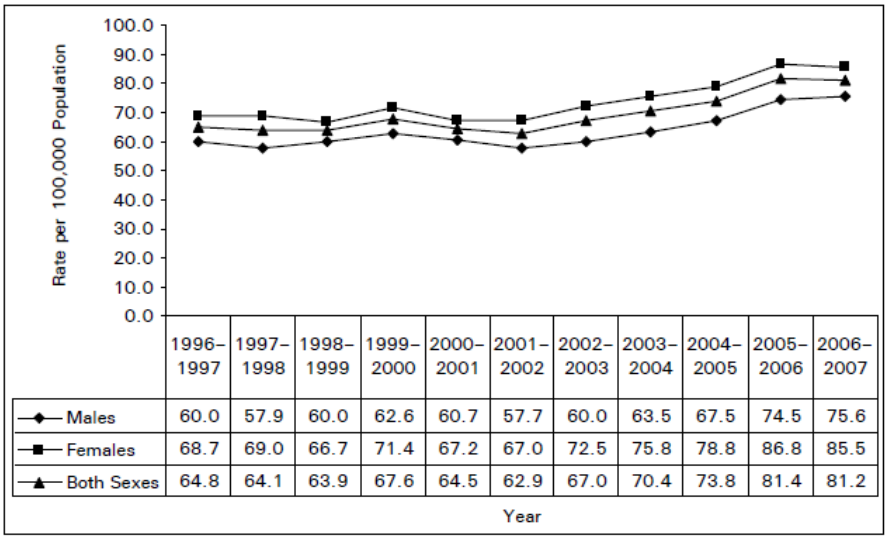

	1996–1997	1997–1998	1998–1999	1999–2000	2000–2001	2001–2002	2002–2003	2003–2004	2004–2005	2005–2006	2006–2007
Males	60.0	57.9	60.0	62.6	60.7	57.7	60.0	63.5	67.5	74.5	75.6
Females	68.7	69.0	66.7	71.4	67.2	67.0	72.5	75.8	78.8	86.8	85.5
Both Sexes	64.8	64.1	63.9	67.6	64.5	62.9	67.0	70.4	73.8	81.4	81.2

Figure 1.20: Age-Standardized Hospitalization Rates (per 100,000 Population) by Sex for Hip Replacement, Canada, 1996–1997 to 2006–2007 [38]

1.17 Implant Material

Materials which are to be used in joint replacement should have several features. They should be biocompatible meaning that they should be able to function within the body without causing any adverse effects. They have to be resistant to corrosion and chemical degradation so that their properties are not affected by the harsh environment within the body. Biomaterials must be strong enough to sustain the large forces that are transmitted across the joints in the body. If such materials are to be used in bearing surfaces such as the acetabular surface, they should be wear resistant over millions of cycles of use without releasing any particulate debris. Finally, biomaterials must be relatively easy to fabricate at a low cost [39]. Some of the most common materials used in joint replacement are as follows:

1.18 Metal Alloys

Metal alloys which are made up of mixtures of metallic and non-metallic elements have high strength, flexibility, ductility, corrosion resistance and biocompatibility to be suitable for load bearing applications as implants in total joint arthroplasty. Three common alloys are used for such a purpose: stainless steel, cobalt-chromium alloy and titanium alloy.

- **Stainless Steel**

Steel is an alloy made of iron and carbon. The properties of steel can be modified in three different ways: the first is by adding elements such as chromium which provides corrosion resistance by forming a strongly adherent oxide film which protects the bulk material from the environment. Steels with high chromium contents are called stainless steels. The second method for improving the property of steel is by heat treatment which increases the strength of the material. Unfortunately this increase is at cost of reducing corrosion resistance. Cold working is another method for improving the properties of stainless steel. For orthopedic applications, stainless steel is usually cold worked by about 30%. The most common type of stainless steel used in orthopedic applications is 316L. This type of stainless steel is mainly used for internal fracture fixation devices [39].

- **Cobalt-Chromium Alloys**

This alloy is composed of cobalt as the base element and a considerable amount of chromium. These alloys are not only relatively easy to fabricate but they have a better resistance to crevice

corrosion compared to stainless steel. The most important problem associated with cobalt alloys is their ability to trap air and gases which escape from the solidification process. This can cause porosity which may in tern become initiation points for fatigue failure [40]

- **Titanium and Its Alloys**

Titanium is used in orthopedic implants in both its pure form or as the base element mixed with other elements in form of alloys. What make titanium alloys suitable for total joint replacement components are their high strength, excellent biocompatibility and corrosion resistance. Corrosion resistance in titanium alloys, unlike stainless steel and cobalt alloys, is provided by an adherent layer of titanium oxide which provides a better resistance to crevice and fretting corrosion. The most commonly used titanium alloy is titanium-aluminum-vanadium alloy. The elastic modulus of this alloy is about half that of stainless steel and cobalt alloys. The axial, bending and torsion stiffness of a hip stem made from titanium alloy is half that of a stem of the same size and shape fabricated from either stainless steel or cobalt alloys. This leads to a reduction in stress shielding for a titanium alloy stem [41]. Despite their advantages, titanium alloys have some major drawbacks. One major disadvantage is notch sensitivity i.e. a stress concentration such as a scratch on the surface of a titanium alloy can greatly reduce the fatigue life of the part [42]. Another limitation of this type of alloy is its low resistance to elastic and plastic deformation which may occur during scratching of a bearing surface.

- **Tantalum**

Tantalum (Ta) is a pure metal with excellent corrosion resistance and biocompatibility. The elastic modulus is 185GPa, yield strength 165GPa, tensile strength 205GPa [43]. It is mainly used as a porous biomaterial to mimic trabecular bone to allow bone ingrowth into the stock. The primary limitation of the use of this implant is the technical challenge in its fabrication.

1.19 Polymers

Polymers are large molecules made from combinations of smaller molecules called mer. The orthopedic applications of polymers are mainly bone cement for the fixation of joint replacement components and polymeric bearing materials especially polyethylene bearing surfaces which have been used successfully in joint arthroplasty for three decades. The most important problem

with these polymeric surfaces is wear debris particle which shortens the life of the total joint replacement [44].

1.20 Ceramics

Ceramics are inorganic compounds which consist of metal and non-metal elements that are held together by ionic or covalent bonding. Like metals, the atomic structure of ceramics is closely packed. Ceramic materials are brittle and very stiff which makes them unsuitable for use in high load applications. However, they are commonly used for two applications in total joint replacement. The first is the usage of fully dense ceramics such as alumina and zirconia as bearing surfaces. The second involves less dense ceramic materials that are used as coatings for metallic implants. These coatings are osteoconductive and provide surfaces to which bone can bond [44].

- **Alumina**

Aluminium oxide which is also called alumina is a good candidate for bearing surfaces in total hip replacement due to its excellent wear and abrasion resistance. Owing to its brittle nature it is used only for the femoral head and acetabular inserts but not for the femoral stem [39].

- **Zirconia**

Zirconia which is another name for zirconium oxide is also used as bearing surfaces for femoral heads due to its low friction surface. However, this material is unstable in its pure form. It may exist in three different phases: tetragonal, monoclinic and cubic arrangement of molecules. Pure zircoina constantly switches in between these three phases which has a detrimental effect on its mechanical properties. For this reason, it is stabilized with yttrium oxide to maintain its most desirable phase which is tetragonal before it can be used for joint replacement [39].

1.21 Bone Resorption in the Femur

It has long been known that inserting a rigid device into bone changes the stress pattern of the bone around the implant. This is due to the stiffness mismatch between implant and the bone. According to Composite Beam Theory, the amount of load carried by each component of the beam depends on the relative structural rigidities of that component. e.g. for a composite beam symmetric about the *x,y* plane consisting of *n* different material components (Figure 1.21) which

is subject to an axial load *P* and a bending moment *M*, the axial stress and bending stress carried by each component are

Axial Stress **Equation 1.9**

$$\sigma_j = \frac{E_j}{\sum_{i=1}^{n} E_i A_i} P$$

Bending Stress **Equation 1.10**

$$\sigma_j = \frac{-E_j}{\sum_{i=1}^{n} E_i I_i} M$$

Where E, A and I represent the modulus of elasticity, cross section area and moment of inertia, respectively. This indicates that the stiffer material bears the bulk of the load preventing the neighboring weaker material from deforming, thus reducing the load on the weaker material. As previously mentioned, this is referred to as stress shielding.

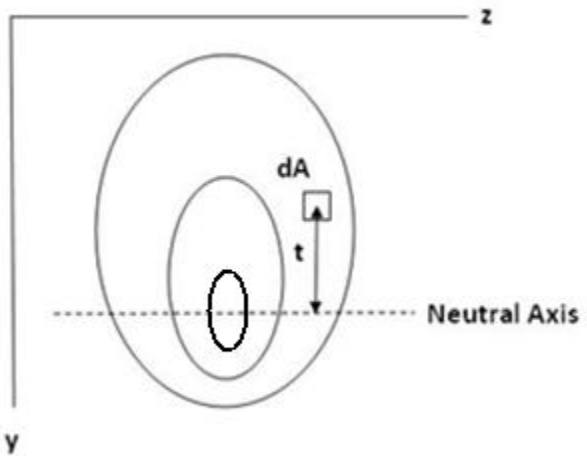

Figure 1.21: The Cross section of a Composite Beam

This is what exactly happens when an implant is inserted into the bone. The implant which is the stiffer component carries the bigger share of the load causing the bone to atrophy and therefore results in bone resorption. This problem was graphically demonstrated in mid-1970's with a canine femoral replacement [45] (Figure 1.22).In general, the extent of stress transfer through the implant depends on a number of factors. It increases with increasing differences between the

implant and the bone stiffness and increasing the rigidity of the connection between them. Another important factor that can affect stress shielding is the load direction. Loading the implant in compression reduces stress shielding because the load is more efficiently transferred to the bone through the implant material, regardless of its stiffness.

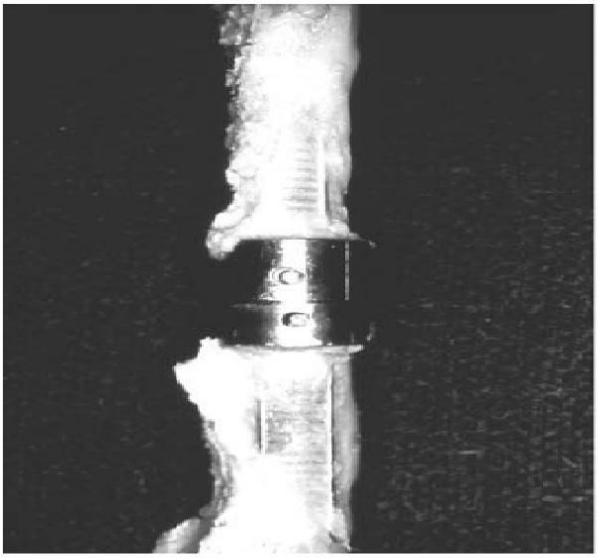

Figure 1.22: Extensive Bone Resorption Because of Stress Shielding Due to Stiffness Mismatch [45]

CHAPTER 2

2 THE THERMODYNAMIC-BASED MODEL FOR BONE EMODELING

2.1 Thermodynamics of Non-equilibrium Processes

According to classical thermodynamics, every system has an internal energy E and entropy S. The change in the entropy of a system may be divided into two parts.

$$dS = dS_i + dS_e \quad \textbf{Equation 2.1}$$

dS_i is the entropy production due to irreversible processes inside the system such as diffusion, heat conduction and chemical reactions. dS_e is the entropy flux due to the exchanges of energy and matter with the environment. The second law of thermodynamics states that the change of entropy within a system due to the occurrence of an irreversible process is always positive i.e.

$$dS_i > 0 \quad \textbf{Equation 2.2}$$

On the other hand, the entropy transfer dS_e can be either positive or negative depending on the direction of the entropy transfer [46].

A non-equilibrium process is referred to a process in which one or more irreversible changes take place which increases the entropy of the system and the surrounding increases. Every irreversible process can be associated a flow J which is produced by a driving force X also known as a thermodynamic force which is usually the gradient in a physical property. For instance temperature gradient is the driving force for heat flow. Concentration gradient is the driving force for mass flow and electric potential is the driving force for the flow of electric charge. The flow of any quantity per unit area is referred to as a flux which is proportional to the driving force [47].

2.1.1 Onsager's First Postulate

If there is only one driving force in a system, there is only one single flow caused by that. Apparently two or more driving forces produce more fluxes. Onsager postulated that these fluxes are coupled. For example, in a single component system the temperature gradient not only produces heat flux but it can also result in a flux of mass so that the total mass flux is a function of not only the concentration gradient but also the temperature gradient. Similarly the heat flux is

a function of both the temperature gradient and the concentration gradient. This Principle can be formulated in the following way [48].

$$J_i = \sum_k L_{ik} X_k$$ **Equation 2.3**

This means that the flux of a property i denoted by J_i is a linear function of all thermodynamic forces, X_k. L_{ik}'s are called the kinetic or Onsager's phenomenological coefficients. In fact, it is already known that the flux J_i is related to the driving force X_i through the coefficient L_{ii}. What this postulate indicates is that other driving forces such as X_k ($i\#k$) also affect J_i through the coefficient L_{ik}.

2.1.2 Onsager's Second Postulate

Onsager's second postulate states that in an irreversible thermodynamic process, the rate of entropy production is equal to the sum of products of fluxes and forces which is formulated as follows: [49]:

$$T(\frac{\partial S}{\partial t}) = \sum_i J_i X_i$$ **Equation 2.4**

2.1.3 Onsager's Third Postulate

Experiments with thermo-elasticity, thermo-diffusion, piezoelectricity and other phenomena which involve the production of a flux by a driving force have revealed that [50]

$$L_{ij} = L_{ji}$$ **Equation 2.5**

This is known as Onsager's third postulate or Onsager's reciprocity relation.

2.2 Chemical Kinetics

2.2.1 Rate of Reaction

For the following hypothetical reaction involving three chemical species *A*, *B* and *C*, the rate of reaction *w* is defined as the slope of the concentration-time plot for a species divided by the stoichiometric coefficient of that species. Additionally, if the species is a reactant, the negative value of the slope is used, because the slope is negative and a positive rate is desired [51].

$$aA + bB \rightarrow cC$$ **Equation 2.6**

$$w = -\frac{1}{a}\frac{d[A]}{dt} = -\frac{1}{b}\frac{d[B]}{dt} = \frac{1}{c}\frac{d[C]}{dt}$$ **Equation 2.7**

2.2.2 Rate Law

The rate law or rate equation is an equation that links the reaction rate with the concentration of the reactants. For the following hypothetical opposite direction reaction, the rate law is expressed as

$$aA + bB \underset{K2}{\overset{K1}{\rightleftarrows}} cC + dD$$ **Equation 2.8**

$$w = k1[A]^a[B]^b - k2[C]^c[D]^d$$ **Equation 2.9**

2.2.3 Affinity of Reaction

Affinity of a chemical reaction (*A*) is the defined as the driving force measured by the decrease in Gibb's free energy (*G*) on going from reactants to products of a chemical reaction [52]:

$$A = -\Delta G = -\Delta(E - TS + pV)$$ **Equation 2.10**

2.3 The Proposed Thermodynamic-Based Model for Bone Remodeling

According to this model, bone is considered as an open thermodynamic system that exchanges matter, energy and entropy with its surroundings. In this open system, bone remodeling takes place as an irreversible process described by 5 chemical reactions. Figure 2.1 shows a schematic representation of bone an open thermodynamic system.

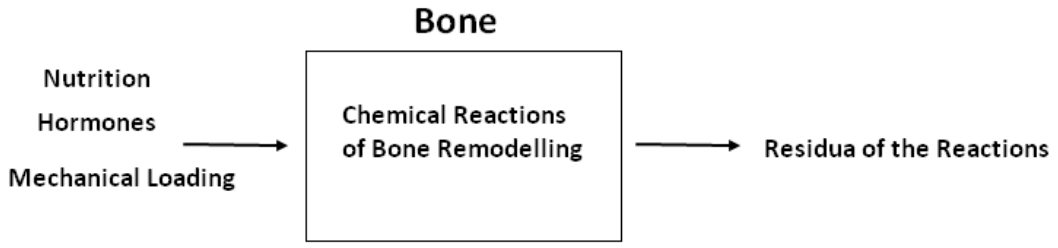

Figure 2.1: schematic representation of bone an open thermodynamic system.

2.3.1 Chemical Reactions in Bone Remodeling

It was previously explained that bone remodeling is the result of the activities of bone cells called osteoblast (responsible for bone formation) and osteoclasts (responsible for bone resorption). Based on the existing knowledge of bone cell regulation and interaction, Bougherara et.al [21] proposed 5 governing chemical reactions to describe the bone remodeling process. In developing these five chemical reactions, it is assumed that the structures in nature are well optimized meaning that products resulting from bone decomposition take part in the formation of the new bone. These chemical reactions are described below:

The bone resorbing cells which are called osteoclasts initially exist as mononuclear cells (*MCELL*). In order to be activated they need to be coupled in multinucleated (*MNOC*) form. The first chemical reaction is the activation of osteoclasts:

$$C1 + MCELL \underset{K-1}{\overset{K+1}{\rightleftarrows}} MNOC + C4$$ **Reaction 1**

C1 the mixture of substances that initiate the reaction with mononuclear cells and *C4* is the remaining product from the reaction. In the next stage of the process, multinucleated osetoclasts act on the bone and break it. This action is described by the following reaction.

$$MNOC + Old\_BONE \underset{K-2}{\overset{K+2}{\rightleftarrows}} C6 + C7$$ **Reaction 2**

C6 and *C7* are the products resulting from the resorption of the bone. Since the process is assumed to be well optimized, part of these products (*C7*) takes in the next stage which is the production of osteoblast activator. Before osteoblasts can carry out their duty which is filling the cavities resulting from bone resoprtion, they need to be activated by an activator which is produced in the following reaction.

$$C7 + Old\_BONE \underset{K-3}{\overset{K+3}{\rightleftarrows}} ACTIVATOR + C9$$ **Reaction 3**

This activator then acts on the osteoblasts (*OB*) to produce osteoid which is the un-mineralized bone.

$$ACTIVATOR + OB \underset{K-4}{\overset{K+4}{\rightleftarrows}} OSTEOID + C12$$ **Reaction 4**

Where *C12* is the product of the fourth reaction. The final stage of bone remodeling is the calcification of the osteoid according to:

$$C13 + OSTEOID \underset{K-5}{\overset{K+5}{\rightleftarrows}} New\_BONE + C15$$ **Reaction 5**

C13 is the substratum that initiates the bone calcification and *C15* is the residue of the bone formation reaction. The above reactions contain 15 chemical substances *C1*, *MCELL*, *MNOC*... *C15* whose concentrations are denoted by n_1, n_2, $n_3 \ldots n_{15}$.

2.3.2 Thermodynamic Description of the Bone Remodeling Process

Klika et.al [53] showed that in a biochemical process which is stimulated by a mechanical stimulus (such as bone remodeling), the reaction rate w_i (a scalar thermodynamic flux) is influenced by the affinity of the i^{th} reaction A_i (a scalar thermodynamic force) and the mechanical pressure p is influenced by the trace of the deformation rate tensor denoted by $d_{(1)}$. Therefore, based on Onsager's first postulate, the cross coupling effect between the mechanical pressure p and chemical reaction rates (w_i) can be expressed as:

$$\begin{aligned} p &= L_{mm} d_{(1)} + L_{mi} A_i \\ w_i &= L_{im} d_{(1)} + L_{ii} A_i \end{aligned}$$ **Equation 2.11**

Where the trace of the deformation rate tensor $d_{(1)}$ is

$$d_{(1)} = \frac{d\varepsilon_{(1)}}{dt} = \frac{d\varepsilon_{ii}}{dt}$$ **Equation 2.12**

Furthermore, if it is assumed that bone remodeling is manly driven by the interaction between the mechanical loading and chemical reactions, the change in the entropy of the system, according to Onsager's second postulate will be

$$T\left(\frac{\partial S}{\partial t}\right) = p d_{(1)} + \sum_{i=1}^{n} w_i A_i$$ **Equation 2.13**

2.3.3 Mathematical Formulation

Time evolution of the concentrations of all the biochemical components involved in the chemical reactions of bone remodeling is described by a set of differential equations which are formulated on the basis of chemical kinetics and non-equilibrium thermodynamics. Based on the definition of reaction rate, the change in the concentration of the chemical components with time can be expressed by the following equation:

$$\dot{n}_i = \sum_{k=1}^{5} (\nu'_{ki} - \nu_{ki}) w_k \qquad \textbf{Equation 2.14}$$

Where the dot indicates differentiation with respect to time. n_i is the concentration of the i^{th} component in the chemical reactions. υ_{ki} is the stoichiometric coefficient of the i^{th} chemical component of the reactants in the k^{th} reaction and υ'_{ki} are stoichiometric coefficients of the i^{th} chemical component of the products in the k^{th} reaction. Taking into account the effect of $d_{(1)}$ on the reaction rate as expressed by Onsager's second postulate, the reaction rate law for each of the five chemical reactions, which describe bone remodeling, is written as follows:

$$w_1 = k_{+1} n_1 n_2 - k_{-1} n_3 n_4 + L_{1m} d_{(1)} \qquad \textbf{Equation 2.15a}$$

$$w_2 = k_{+2} n_3 n_5 - k_{-2} n_6 n_7 + L_{2m} d_{(1)} \qquad \textbf{Equation 2.15b}$$

$$w_3 = k_{+3} n_7 n_5 - k_{-3} n_8 n_9 + L_{3m} d_{(1)} \qquad \textbf{Equation 2.15c}$$

$$w_4 = k_{+4} n_8 n_{10} - k_{-4} n_{11} n_{12} + L_{4m} d_{(1)} \qquad \textbf{Equation 2.15d}$$

$$w_5 = k_{+5} n_{11} n_{13} - k_{-5} n_{14} n_{15} + L_{5m} d_{(1)} \qquad \textbf{Equation 2.15e}$$

Inserting Equations 2.14 into Equation 2.13 yields a set of differential equations. These differential equations can be in dimensionless form by scaling the variables according to [21]:

$$\tau = t k_{+2} n_{B0} \qquad N_i = \frac{n_i}{n_{B0}} \qquad \delta_i = \frac{k_{+i}}{k_{+2}}$$

$$\beta_i = \frac{B_i}{n_{B0}} \qquad D_i = \frac{l_{iv} d_{(1)}}{k_{+2} n^2{}_{B0}} \qquad J_i = \frac{j_i}{k_{+2} n^2{}_{B0}} \qquad \textbf{Equation 2.16}$$

Where t is time, δ_i is the ratio of the rate of the i^{th} reaction to the second reaction; j_i is the flux of the i^{th} substance. n_{B0} is the sum of the initial molar concentration of the relevant substances which are *MCELL, Old_BONE, ACTIVATOR, OSTEOID* and *New_BONE* . D_i is the influence of the strain rate on the rate of the i^{th} chemical reaction in dimensionless form. The B_i's are defined as follows [21]:

$$B_1 = n_1 - n_2 \quad \textbf{Equation 2.17a}$$

$$B_3 = n_3 + n_2 - n_5 - n_8 - n_{11} - n_{14} \quad \textbf{Equation 2.17b}$$

$$B_7 = n_7 + n_5 + 2n_8 + 2n_{11} + 2n_{14} \quad \textbf{Equation 2.17c}$$

$$B_{10} = n_{10} + n_{11} + n_{14} \quad \textbf{Equation 2.17d}$$

$$B_{13} = n_{13} + n_{14} \quad \textbf{Equation 2.17e}$$

Time evolution of the concentrations of relevant substances in dimensionless form will therefore be:

$$\dot{N}_{MCELL} = \frac{\partial N_{MCELL}}{\partial \tau} = -\delta_1(\beta_1 + N_{MCELL})N_{MCELL} + J_3 + J_{New\_B} - D_1 \quad \textbf{Equation 2.18a}$$

$$\dot{N}_{Old\_B} = \frac{\partial N_{Old\_B}}{\partial \tau} = -\big(\beta_3 - N_{MCELL} + N_{Old\_B} + N_{Activ\_B} + N_{Osteoid} + N_{New\_B}\big)N_{Old\_B} - \delta_3\big[\beta_7 - N_{Old\_B} - 2\big(N_{Activ\_OB} + N_{Osteoid} + N_{14}\big)\big]N_{Old\_B} + 2J_{New\_B} - D_2 - D_3 \quad \textbf{Equation 2.18b}$$

$$\dot{N}_{Activ\_B} = \frac{\partial N_{Activ\_B}}{\partial \tau} = \delta_3(\beta_7 - N_{Old\_B} - 2\big(N_{Active\_B} + N_{Osteoid} + N_{New\_B}\big)N_{Old\_B} - \delta_4\big(\beta_{10} - N_{Osteoid} - N_{New\_B}\big)N_{Active\_OB} + D_3 - D_4 \quad \textbf{Equation 2.18c}$$

$$\dot{N}_{Osteoid} = \frac{\partial N_{Osteoid}}{\partial \tau} = \delta_4\big(\beta_{10} - N_{Osteoid} - N_{New\_B}\big)N_{Activ\_OB} - \delta_5(\beta_{13} - N_{New\_B})N_{Osteoid} + D_4 - D_5 \quad \textbf{Equation 2.18d}$$

$$\dot{N}_{New\_B} = \frac{\partial N_{New\_B}}{\partial \tau} = \delta_5(\beta_{13} - N_{New\_B})N_{Osteoid} - J_{New\_B} + D_5$$ **Equation 2.18e**

Solution to the above-mentioned differential equation will yield the concentration of the relevant substances as follows [21]:

$$N_{MCELL} = 0.5\left(-\beta_1 + \sqrt{\beta_1^{\,2} + 4\frac{-D_1 + J_3 + J_{14}}{\delta_1}}\right)$$ **Equation 2.19a**

$$N_{OLDBONE} = 0.5\left(\frac{-(\beta_7 + 2\beta_3 - 2N_{MCELL}) + }{\sqrt{(\beta_7 + 2\beta_3 - 2N_{MCELL})^2 + 4\left(\frac{J_{14} - D_3}{\delta_3} + 2J_{14} - 2D_2\right)}}\right)$$ **Equation 2.19b**

$$N_{ACTIVATOR} = 0.5\left(\frac{-(\beta_{10} + 0.5\left(N_{OLDBONE} - \beta_7 + \frac{J_{14} - D_3}{\delta_3 N_{OLDBONE}}\right)) + }{\sqrt{(\beta_{10} + 0.5\left(N_{OLDBONE} - \beta_7 + \frac{J_{14} - D_3}{\delta_3 N_{OLDBONE}}\right))^2 + 4\frac{J_{14} - D_4}{\delta_4}}}\right)$$ **Equation 2.19c**

$$N_{OSTEOID} = 0.5\left(\frac{-(\beta_{13} - \beta_{10} + \frac{J_{14} - D_4}{\delta_4 N_{ACYTIVATOR}}) + }{\sqrt{(\beta_{13} - \beta_{10} + \frac{J_{14} - D_4}{\delta_4 N_{ACTIVATOR}})^2 + 4\frac{J_{14} - D_5}{\delta_5}}}\right)$$ **Equation 2.19d**

$$N_{NEWBONE} = -N_{OSTEOID} + \beta_{10} - \frac{J_{14} - D_4}{\delta_4 N_{ACTIVATOR}}$$ **Equation 2.19e**

2.3.4 Density and Elastic Moduli of the Bone

The density of the bone is related to the initial density ρ_0 and the normalized concentrations of the new and old bones (calculated from Equation 2.18) according to the following law of mass and mixture [54].

$$\rho = \rho_0 \left(N_{OLDBONE} + N_{NEWBONE} \right) \quad \textbf{Equation 2.20}$$

The elastic modulus is calculated using the empirical power law relationship proposed by Carter et.al. [55].

$$E = \left(E_{OLDBONE} \left[\frac{N_{OLDBONE}}{N_{OLDBONE} + N_{NEWBONE}} \right] + E_{NEWBONE} \left[\frac{N_{OLDBONE}}{N_{OLDBONE} + N_{NEWBONE}} \right] \right) \left(\frac{\rho}{\rho_0} \right)^3 \quad \textbf{Equation 2.21}$$

2.3.5 Calculation of the Effect of Strain Rate

ANSYS Finite Element Software calculates only the deformation, so the strain trace which is the sum of the principal strains can be calculated in each element of the bone. In order to determine the rate of the deformation tensor $d_{(1)}$ for each element, the following relation is applied:

$$d_{(1)}(I) = \frac{d\epsilon_{(1)}(I)}{dt} \approx \frac{\Delta\epsilon_{(1)}(I)}{\Delta t} \approx \frac{\epsilon_{(1)}(I)}{\Delta t} \quad \textbf{Equation 2.22}$$

Where ε (I) is the trace of strain in the element I. The above-mentioned relation is based on the assumption that the finite elements are small enough so that the change in the strain between two consecutive time intervals is approximately equal to the strain itself. Since the constants which relate the effect of strain rate *D* to $d_{(1)}$ are more or less still unknown, it can be assumed, based on Hook's law, that a linear relationship exists between the influence *D* and $d_{(1)}$ [21].

$$D_\rho(I) = C d_{(1)}(I) \quad \textbf{Equation 2.23}$$

Where *C* is a constant defined as the ratio of the reference strain rate on the i^{th} chemical reaction and the reference strain rate.

$$C = \frac{D_\rho(ref)}{ref\_strain\_rate} \quad \textbf{Equation 2.23}$$

The value of the reference strain rate is between 0.01 and 0.1 [56].The combination of Equations 2.23 and 2.24 yields:

$$D_\rho(I) = \frac{|d_{(1)}(I)|}{(refref\_strain\_rate)} D_\rho(ref) = \frac{1}{\Delta t} \frac{|\epsilon_{(1)}(I)|}{ref\_strain\_rate} D_\rho(ref)$$ **Equation 2.24**

It should be noted that since both compressive and tensile loading have the same effect on bone remodeling [56], the absolute value of the strain is used.

2.4 Finite Element Implementation

In this work the thermodynamic model, described above, is implemented into the FEM Software ANSYS 11.0 through a user-defined macro in the ANSYS Parametric Design Language (APDL). Once the geometry is imported into ANSYS, it is discretized and the loads are applied. The finite element analysis yields the trace of strain $\varepsilon_{(1)}$ for each element which in turn gives the value for D_i's through Equation 2.24. The D_i's are then plugged into Equation 2.19 to obtain the values for $N_{OLDBONE}$ and $N_{NEWBONE}$ for each element. Using Equations 2.20 and 2.21, the density and elastic modulus are calculated for each element. These new material properties are then assigned to the finite element model of the bone and the process is repeated. Convergence of this iterative process is considered when no significant change in the density of the elements is observed which is determined using the following convergence criterion:

$$CONV = \frac{1}{n} \sum_{i=1}^{n} \left| \rho_i^{(t)} - \rho_i^{(t-1)} \right|$$ **Equation 2.25**

Where n is the number of elements. In the present study, it is assumed that convergence is reached when CONV<0.0001. Figure 2.2 shows the iterative process of the thermodynamic bone remodeling.

Table 2.1 lists the values for the biological and chemical parameters used in the present analysis. Due to lack of experimental facilities these parameters were obtained through adjustment in accordance with clinical observations.

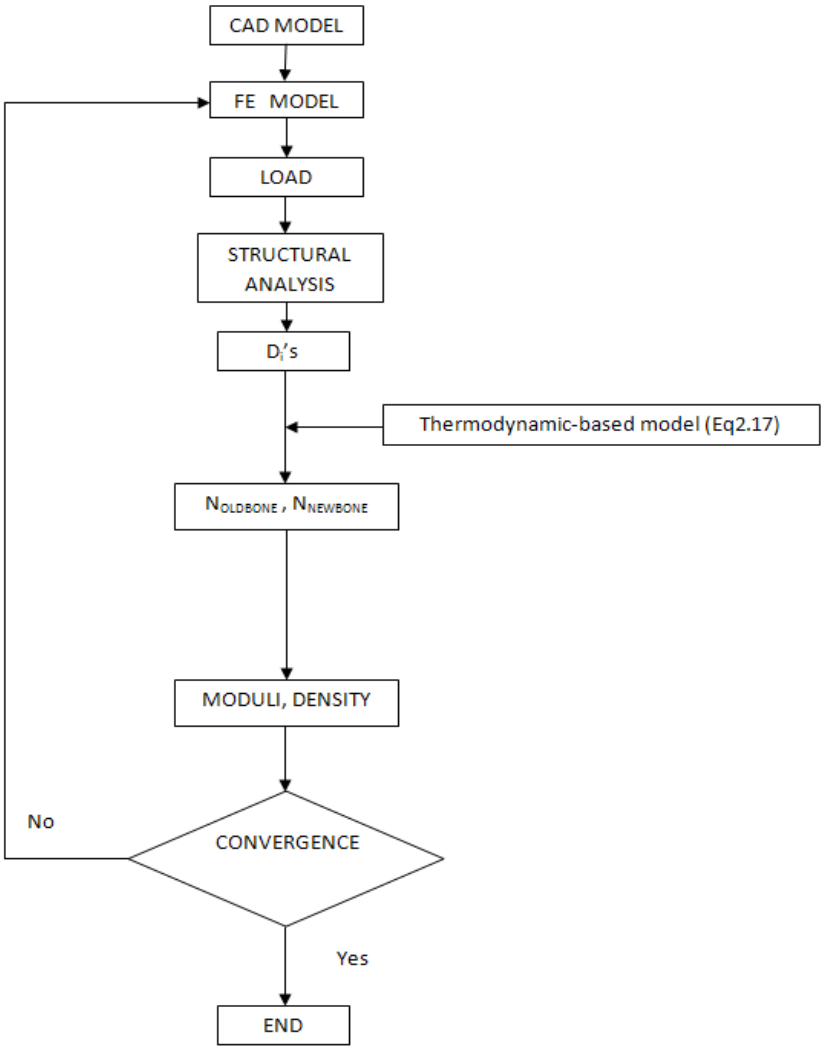

Figure 2.2: The Iterative Process of the Thermodynamic Bone Remodeling

$E_{OLDBONE}$ *(MPa)=21*	$\beta_{3=}$*24.10*	J_3*=2.38*	δ_4*=5.75*	D_3*(ref)=5.85*
$E_{NEWBONE}$ *(MPa)=14*	$\beta_{7=}$*4.85*	J_{14}*=5.07*	δ_5*=3.08*	D_4*(ref)=1.30*
ρ_0 *(gr/cm^3)=1*	$\beta_{10=}$*2.28*	δ_1*=20.29*	D_1*(ref)=2.44*	D_5*(ref)=4.68*
$\beta_{1=}$*5.23*	$\beta_{13=}$*3*	δ_3*=10.03*	D_2*(ref)=1.26*	Δt *(sec)=1*

Table 2.1: The List of Parameters Used in the Analysis [21]

CHAPTER 3

3 FINITE ELEMENT MODELLING

3.1 CAD Modelling

3.1.1 Femur

The fourth generation composite femur model is fully scanned using computed tomography (CT). CT scanning is a non-desctructive imaging technique, whereby focused X-ray beams are projected on the target object. Detectors situated around the test subject measure the instensity of these beams once they have passed through the subject, and develop an image where the pixel intensity of a region is directly proportional to the intensity of the beam once it radiates through the corresponding location on the subject. A series of 2D X-ray images were taken, scanned across all three of the body planes (coronal, sagittal, and axial). Cross sectional images across each plane are thus obtained at every 0.5 mm along the length of the femur model. A total of 789 images are obtained. The images are stored in the DICOM format (Digital Imaging and Communications in Medicine). 'Stacking' these cross sectional images reveals a complete 3D internal and external geometry. The cross section images in the DICOM format are imported into Mimics® Medical Imaging Software (The Materialise Group, Leuven, Belgium), which can produce a 3D image from the CT images.

Mimics is used for image segmentation, whereby each image 'slice' is stacked according to shared boundaries between bones and cavities. A connectivity algorithm ensures that the geometry of adjacent slices are free of discontinuities, and a subsequent 3D model is developed. The model is then saved in its triangulated surface geometry version as an STL (*.stl, stereolithography) file. The file contained geometry data for both the outer cortical layer and inner cancellous bone surfaces. The model is imported into Geomagic Studio (Geomagic, Inc., Research Triangle Parck, NC, USA), where the polygon surface model is optimised. At this stage, the model contains a few 'holes' or cavities in places where the CT scanning or the subsequent segmentation phase could not obtain sufficient surface detail . These holes are manually healed on both cortical and cancellous surfaces (external and internal surfaces).At this point, the surfaces are rough, populated with small 'ridges and bumps'. Surface smoothening is

performed in the software by alternately using a 'Relaxation' utility and an inbuilt surface curvature curing algorithm, which results in an improvement in the surface finish. Surface grid patterns are generated and checked for errors which are corrected. The model is then saved as an IGES (*.igs, Initial Graphics Exchange Specification), and imported into ANSYS Workbench 11.0 (ANSYS, Inc., Canonsburg, PA, USA). Using Workbench, the cortical-cancellous geometry is processed to produce two separate solids using the 'Slice' utility. The compound solid is then exported in the Parasolid Binary format (*.x_b; Siemens PLM Software, Siemens AG, Berlin and Munich, Germany) to SolidWorks 2008 (SolidWorks Corp., Dassault Systèmes, Concord, MA, USA). The surface topography is further improved in SolidWorks which yields the final femur geometry as shown in Figure 3.1.

Figure 3.1: Full Femur Final CAD Model [57]

3.1.2 Implants

The implant geometries were also developed using SolidWorks. The implant components and the bone geometry were assembled to replicate the experimental setup. To generate the complex geometry of the Omnifit Eon stem, NextEngine 3D scanner (NextEngine, Inc, Santa Monica, CA, USA) was employed. This scanner can quickly create highly detailed, full colour, digital models measuring at a speed of 50,000 points per second with multi-laser precision. These CAD models were later imported into the Finite Element software ANSYS 11.0 for analysis.

3.2 The Finite Element Method

A wide variety of theories and exact solution methods are available in classical mechanics for certain classes of structures. Finite element method (FEM), however, is a numerical method which is suitable for any structures, geometries, and material properties and loading of arbitrary

complexity. In this method, the geometry is first defined in terms of a Computer Aided Design (CAD) model. This CAD model is then discretized into a number of small but finite sized elements. These elements are connected at specific geometric points called nodes. The boundary conditions and loads are numerically defined as displacement and/or forces at these nodes. Every element has to be assigned one or more parameters such as the moduli of elasticity that define its material properties. A computer program calculates the stiffness characteristics of each element and assembles the element mesh through mutual forces and displacements in each node. As a matter of fact, the FEM program solves a large number of equations that govern force equilibrium at element nodes. The computational time needed for an FEM analysis depends not only on the number of elements but also on the type of the elements used. The solution obtained through a FEM analysis is an approximate solution which converges to the exact solution when the number elements approach infinity. A variety of element types are available for one, two and three dimensional analyses in Finite Element computer packages.

3.3 Early Works of FE Applications in THA

Since the mechanical stimulus for bone remodeling is the change in bone's strain, bone remodeling algorithms can be incorporated into finite element models in order to calculate the strain. The strain values are then related to bone density. The material properties in these finite element models are expressed as a function of density. Therefore the application of the load in an iterative process causes the bone density to change. This process will go on until no sensible change in the density between two consecutive processes takes place. Finite element method is well-suited to model bone's irregular geometry and its varied material properties and loading. Artificial joint design and fixation is probably the most popular application of FEM in orthopedic biomechanics. The mechanical problems involved in joint implants are very challenging both because of the long expectancy and the severe loading conditions imposed within the body. Failure mechanisms in joint implants include plastic deformation and fatigue fracture of metal and plastic components due to the cyclic loading condition on the implant. There is also the problem of the breakdown of the acrylic cement (used to fix the prosthesis to the bone), loosening at the boundaries between different materials and also the stress shielding issue. Other problems involve unknown loading and boundary conditions and the wide variation among patient population due to specific pathologies and different surgical procedures performed [58].

The first two dimensional FE models of the femoral hip prosthetic component were analyzed by Andriacchi et al. [59], Kwak et al. [60], Yettram and Wright [61], Cook et al. [62], Sih et al. [63] and Skinner et al. [64]. Axisymmetric geometry applying three dimensional elements was developed by Huiskes et al [65]. The majority of theses FEM analyses assumed linear elasticity, isotropy and homogeneity of the cortical and trabecular bone, whereas interfaces were modeled as rigidly bonded. The anisotropy of the cortical bone was investigated in the work of Valliappan et al. [66]. Ever since 1975, a lot of FE analyses on hip joint prostheses have been conducted. Recently, multiscale finite element method which (unlike conventional finite element method which models bone as a continuum) is capable of modeling the microstructure of the bone as a porous medium has been implemented to predict the failure of implants [67].

3.4 Element Types

The three dimensional finite element models were constructed and analyzed using ANSYS 11.0. Fully bonded conditions were assumed at all interfaces considering the interfacial adhesion measured from pull tests. Three types of elements were used in the finite element analysis.

3.4.2 SOLID187 3-D 10-Node Tetrahedral Structural Solid

SOLID187 is included in ANSYS Workbench which has a higher order 3D tetrahedral solid element. All the solid bodies were modeled with this element. This element has three degrees of freedom at each node, having 10 nodes, in the nodal x, y, and z directions. Its behavior is quadratic displacement, and is quite well to modeling irregular meshes like those imported from CAD software, and because of this quality SOLID187 has been used to model the highly curvaceous geometry of the implant components. This element has plasticity, hyper elasticity, creep, stress stiffening, large deflection, and large strain capabilities. Moreover, it has mixed formulation capability for simulating deformations of nearly incompressible elastoplastic materials, and fully incompressible hyper elastic materials. This element would be ideal if used for further analysis, in future, for FE model of this study including the more complex material behavior. This element input data includes the orthotropic or anisotropic material properties, which correspond to the element coordinate directions. Figure shows the node locations, the coordinate system, and the geometry for this element. Figure illustrates the element stress directions which are parallel to the element coordinate system, and the surface stress outputs are in the surface coordinate system [68].

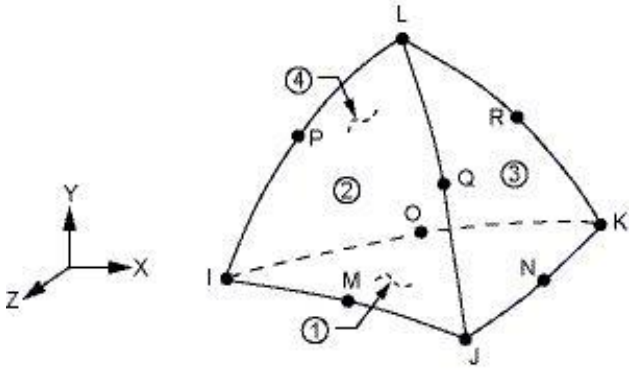

Figure 3.2: SOLID187 Element Description [68]

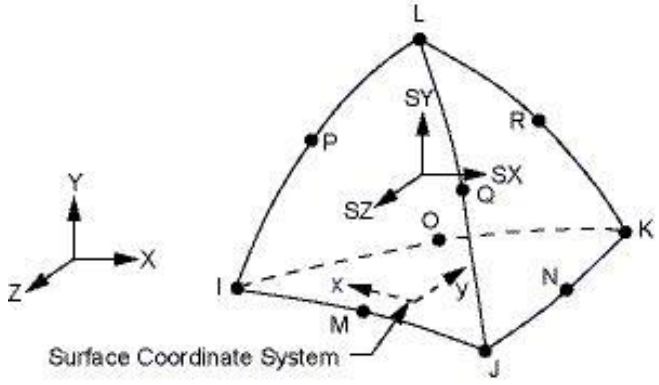

Figure 3.3: SOLID187 Stress Output Directions [68]

3.4.3 TARGE170 3D Target Segment

To represent various 3-D "target" surfaces for the associated elements, TARGE170 is used. The contact elements themselves overlay the solid, shell, or line elements describing the boundary of a deformable body and are potentially in contact with the target surface, defined by TARGE170. The target surface is discretized by a set of target segment elements (TARGE170) and is paired with its associated contact surface via a shared real constant set. For rigid target surfaces, these elements can easily model complex target shapes. For flexible targets, these elements will overlay the solid, shell, or line elements describing the boundary of the deformable target body .Each target surface can be associated with only one contact surface, and vice-versa. However, several contact elements could make up the contact surface and thus come in contact with the same target surface. In the same way, several target elements could make up the target surface and thus come in contact with the same contact surface. For either the target or contact surfaces,

many elements may be applied in a single target or contact surface, but doing so may increase computational cost. For a more efficient model, localize the contact and target surfaces by splitting the large surfaces into smaller target and contact surfaces, each of which contain fewer elements. If a contact surface contacts more than one target surface, duplicate contact surfaces must be defined that share the same geometry but relate to separate targets that have separate real constant set numbers [69]. Figure shows the element description for TARGE170.

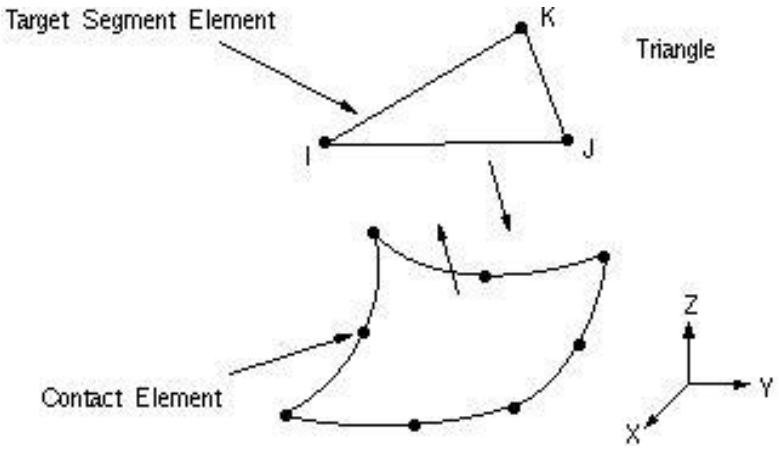

Figure 3.4: TARGE170 Element Description [68]

3.4.4 SHELL99 Linear Layered Structural Shell

SHELL99 may be used for layered applications of a structural shell model. The element has six degrees of freedom at each node: translations in the nodal x, y, and z directions and rotations about the nodal x, y, and z-axes. The geometry, node locations, and the element coordinate system for this element are shown in Figure 3.5. The element is defined by eight nodes, average or corner layer thicknesses, layer material direction angles, and orthotropic material properties. Midside nodes may not be removed from this element. Each layer of the laminated shell element may have a variable thickness which may be input at the corner node locations. If the layer has a constant thickness, only the thickness of node I need be input. If the thickness is not constant, all four corner thicknesses must be input using positive values. The total thickness of each shell element must be less than twice the radius of curvature, and should be less than one-fifth the radius of curvature. You can specify the nodes to be at the top, middle or bottom surface of the element [70].

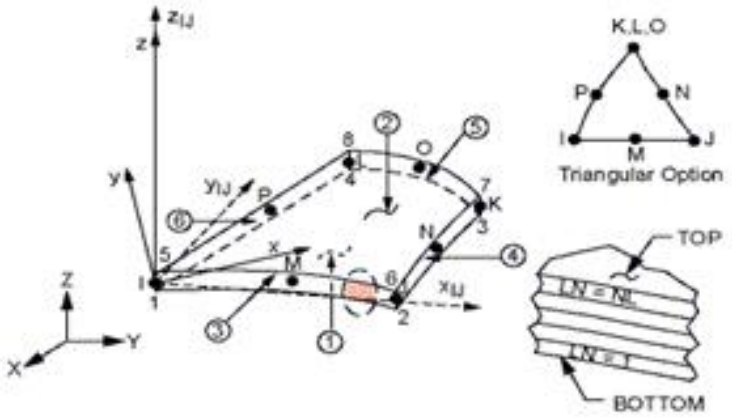

Figure 3.5: Shell99 Element Description [68]

3.5 Mesh Sensitivity

The CAD models are meshed using ANSYS Workbench. The same geometries as the ones used in the present work have already been tested for mesh sensitivity. It has been shown that convergence is achieved at a mesh relevance of 85% [69-71]. However, in the present study a mesh relevance of 100% is used to generate the finite element models.

3.6 The Femoral Bone

The cancellous and cortical bones were modeled using Solid187 finite elements. The material properties of cancellous and cortical bones are listed in Table 3.1. Figure 3.6 shows the finite element model of the intact femur which consists of 10236 elements and 16976 nodes.

Bone Type	**Modulus of Elasticity** (MPa)	**Poisson Ratio** (ν)
Cancellous	2000	0.3
Cortical	16000	0.3

Table 3.1: The Properties of Cancellous and Cortical Bones [72]

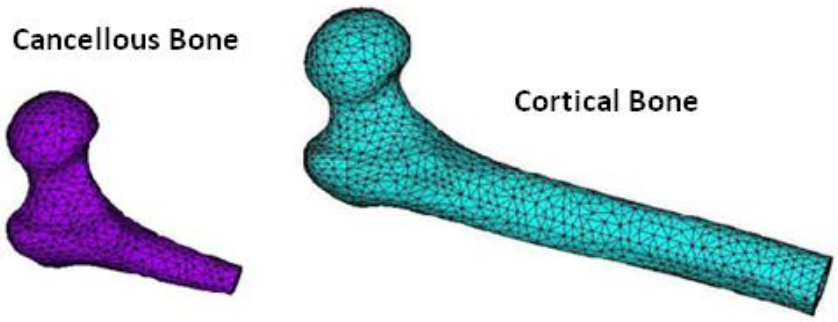

Figure 3.6: The FE Model of the Intact Femur

3.7 The Conventional Titanium Implant

The stem follows the natural curve of femoral bone and has an oval cross-section, a shaft angle of 135 *deg*, a wall thickness of 3 *mm*, an overall length of 230 *mm*, a maximum diameter of 30.3 *mm* at the proximal base of the neck, and a minimum diameter of 15.8 mm at the distal tip. The titanium implant is modeled analyzed using Solid187 finite elements. The material properties of the titanium implant are listed in Table 3.2. The finite element model of the titanium implant consisting of 14966 elements is shown in Figure 3.7.

Implant	**Modulus of Elasticity** (MPa)	**Poisson Ratio** (ν)
Titanium	110000	0.3

Table 3.2: The Properties of Titanium Implant [72]

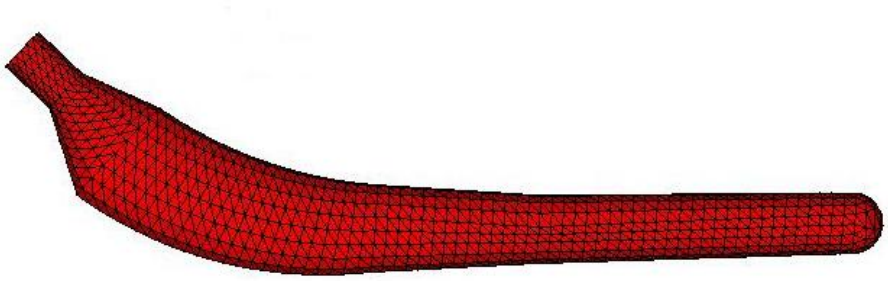

Figure 3.7: The FE Model of the Conventional Titanium Implant

3.8 Stryker Exeter Implant

The Stryker Exeter hip stem (size 2, offset 37.5*mm*) (Stryker, Mahwah, NJ, USA) consists of a single piece of cobalt-chromium-molybdenum (CoCrMo) alloy material. The material properties of the Stryker Exeter implant are listed in Table 3.3. The finite element model of the Stryker Exeter implant consisting of 4573 elements is shown in Figures 3.8.

Implant	**Modulus of Elasticity** (MPa)	**Poisson Ratio** (ν)
CoCrMo Alloy	210000	0.3

Table 3.3: The Properties of Stryker Exeter Implant [73]

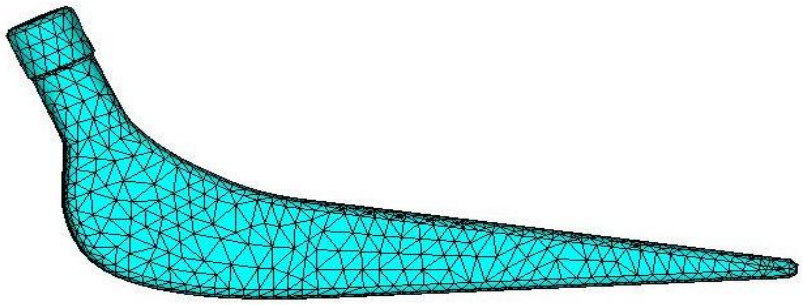

Figure 3.8: The FE Model of the Stryker Exeter Implant

3.9 Stryker Omnifit Eon Hip Implant

The Stryker Omnifit Eon hip stem (Size 7, offset 41mm) (Stryker, Mahwah, NJ, USA) is comprised of a single piece of titanium alloy (Ti-13Nb-13Zr and Ti-29Nb-13Ta-4.6Zr) which provides sufficient strength and corrosion resistance. This type of alloy has a much lower modulus of elasticity compared to the conventional Ti-6Al-4V alloy which in turn reduces stress shielding enhance bone remodeling. These materials have high cost, inferior wear properties. Table 3.4 shows the material properties of this type of titanium based alloy. The finite element model of the Stryker Omnifit implant consisting of 13746 elements is shown in Figure 3.9.

Implant	Modulus of Elasticity (MPa)	Poisson Ratio (ν)
Titanium Based Alloy	80000	0.3

Table 3.4: The Properties of Stryker Omnifit Implant [73]

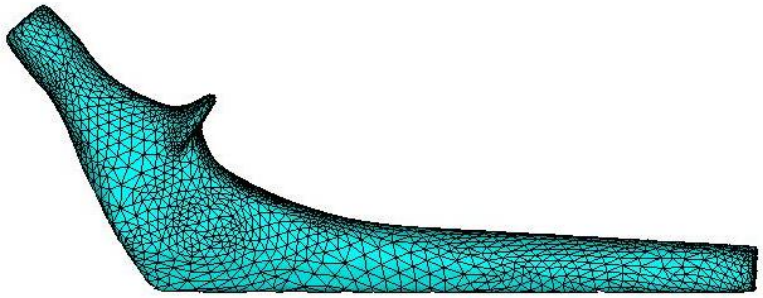

Figure 3.9: The FE Model of the Stryker Omnifit Implant

3.10 Composite (CF/PA12) Hip Stem

The stem follows the natural curve of femoral bone and has an oval cross-section, a shaft angle of 135 *deg*, a wall thickness of 3 *mm*, an overall length of 230 *mm*, a maximum diameter of 30.3 mm at the proximal base of the neck, and a minimum diameter of 15.8 mm at the distal tip.It can be seen that the overall shape of this implant is the same as the conventional titanium hip stem. It is composed of a 3 *mm* thick composite layer made of carbon fiber (CF)/polyamide 12 (PA12) and an internal polymeric core. A 100 micrometer bioactive HA coating is wrapped around the proximal section to establish a better connection with the bone and improve the fixation strength. The material properties of the composite implant are listed in Table 3.5. The polymeric core is meshed using 11126 solid elements and the composite layer is meshed with 3015 Shell99 finite elements as shown in Figure 3.10.

Material	Modulus of Elasticity (MPa)	Shear Modulus (MPa)	Poisson's Ratio
CF/PA12 **$[\pm 45]_6$**	$E_x = 15400$	$G_{xy} = 3000$	$\nu_{xy} = 0.3$
	$E_y = 15400$	$G_{xz} = 3500$	$\nu_{xz} = 0.25$
	$E_z = 3500$	$G_{yz} = 3200$	$\nu_{yz} = 0.2$
Polymeric Core	$E = 600$	$G = 2500$	$\nu = 0.2$

Table 3.5: The Properties of Composite Implant [9]

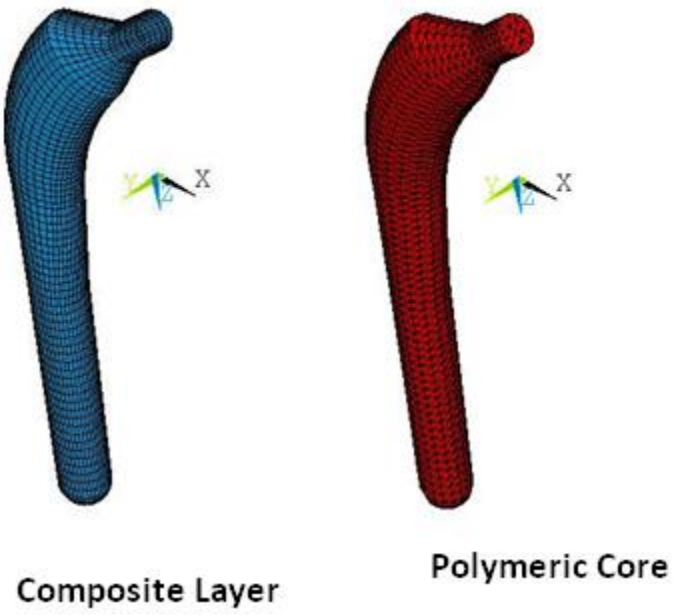

Figure 3.10: The FE Model of the Composite Implant

3.11 Loading and Boundary Conditions

Three loading cases on the femur are considered here. Load case 1 corresponds to the loading condition for the midstance phase of gait. Load cases 2 and 3 represent the extreme cases of abduction and adduction, respectively. These loading cases are defined in Table 3.6. In this study

a superposition of the 3 load cases is applied in order to represent and average daily loading situation [69]. Each of these load cases is distributed over several nodes in order to avoid stress concentration and the displacement of all the nodes at the distal end of the femur is constrained to prevent rigid body motion. Figure 3.11 shows a schematic illustration of these load cases on the implant.

Load Case	Type of Loading	Joint Force	Load Angle	Muscle Force	Load Angle
1	**Midstance Phase of Gait**	2.317 *kN*	240	0.703 *kN*	280
2	**Extreme Range of Abduction**	1.158 *kN*	-150	0.351 *kN*	-80
3	**Extreme Range of Adduction**	1.548 *kN*	560	0.468 *kN*	350

Table 3.6: Loading Condition on the Femur [72]

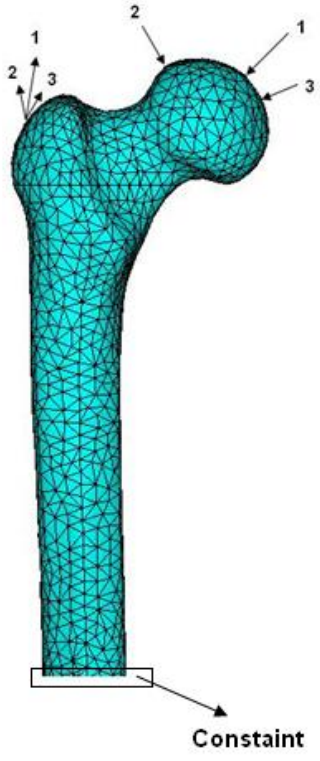

Figure 3.11: Load Cases 1, 2 and 3 on the Femur

CHAPTER 4

4 RESULTS AND DISCUSSION

4.1 Convergence

The remodeling process in the present analysis is controlled by the convergence criterion described by Equation 2.25. As can be seen in Figure 4.1, the convergence of the calculated results for the remodeling of the intact femur and the femoral bone around the conventional titanium hip stem is obtained after almost 80 iterations. It is observed that 80 iterations can result in convergence for other implants, as well.

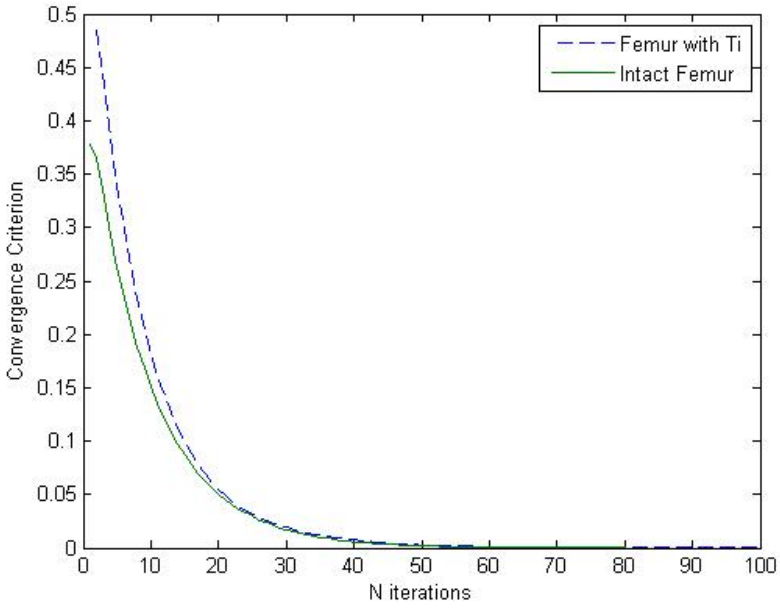

Figure 4.1: Convergence of the Remodeling Process

4.2 Verification

4.2.1 Intact Femur

Figure 4.2 shows the density distribution in the proximal femur compared to clinical observation (adapted with permission from Truong et al. [74]). It is clear from the figure that the development of a dense cortical bone around the medullary canal and a dense trabecular bone between the femoral head and calcar region of the medial cortex is due to compressive stresses.

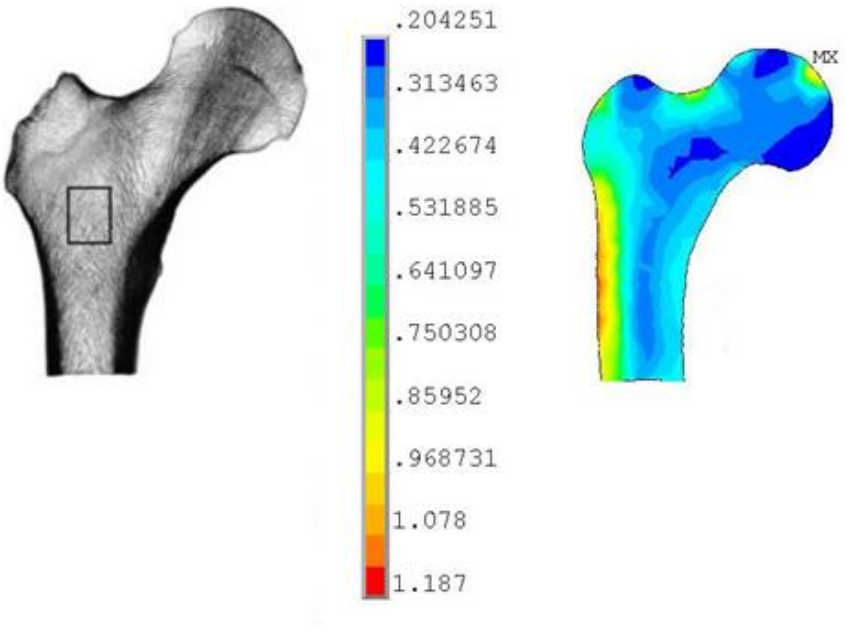

Figure 4.2: Bone Density Distribution (g/cm^3) X-ray of a Healthy Femur [74] (Left), Intact Femur (Right)

Weinans et al. [75] investigated the density distribution of the bone for different femoral stem materials using the strain energy model in combination with the finite element method. Figure 4.3 compares the density distribution of the intact femur obtained from the present analysis with that of reference [75] which is based on the strain energy model. It should be noted that in the strain energy model the bone density distribution strongly depends on the upper and lower limits of the density which in this case are 0.01 g/cm^3 and 1.74g/cm^3. Nevertheless, the patterns of the density distribution in both models are to some extent similar. Like the previous figure, in both models, the development of dense cortical bone in the proximal/lateral region and an area of rather dense trabecular bone between the femoral head and the calcar region of the medial cortex due to compressive loading are observed. There is also a region of high density on the neck of the femur between the head and the greater trochanter due to the bending load. The discrepancy between the two models can be attributed to the differences in geometries which can affect the load distribution. In addition, the finite element model in the present study is three dimensional compared to the two dimensional model of the literature.

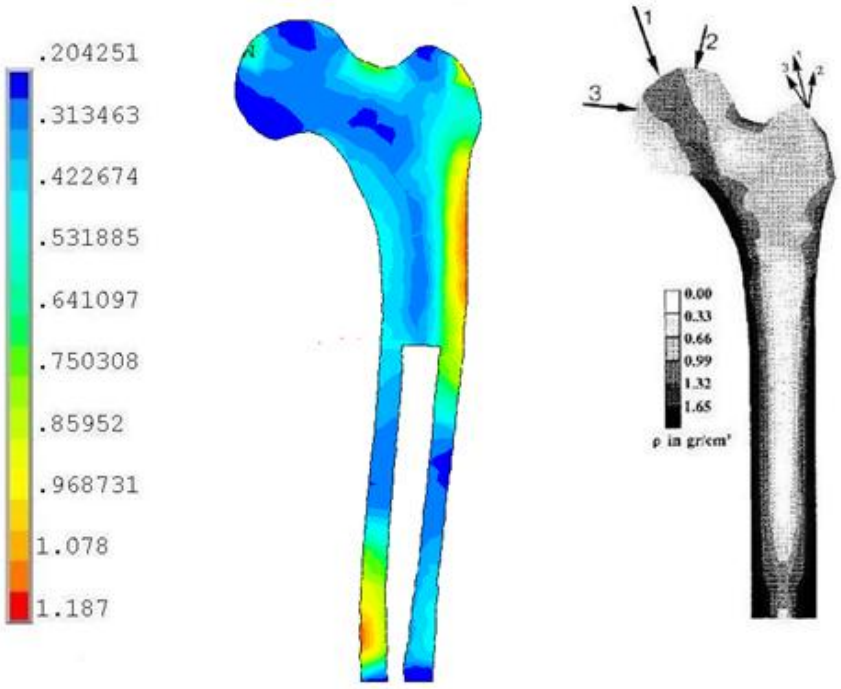

Figure 4.3: Intact Femur Density Distribution (g/cm^3) Present Analysis (Left), Literature [75] (Right)

4.2.2 Femur with Implant

In order to study the bone distribution around the implant, the density of the intact bone at equilibrium was used as the starting point for THR simulation. Figure 4.4 compares the density distribution of the proximal femur around the Omnifit geometry (which is the closest shape to the implant used in the literature) with titanium material properties implant obtained from the thermodynamic model with that of the literature. It should be emphasized that the most important issue after total hip arthroplasty is to minimize load transfer to the distal part of the femur due to the difference between the stiffnesses of the implant and the bone. That's why examining the density distribution in the proximal area of the femur can be a good indication of the extent of load transfer to the distal part i.e. less resorption in the proximal femur implies less load transfer to the distal part which means reduced stress shielding.

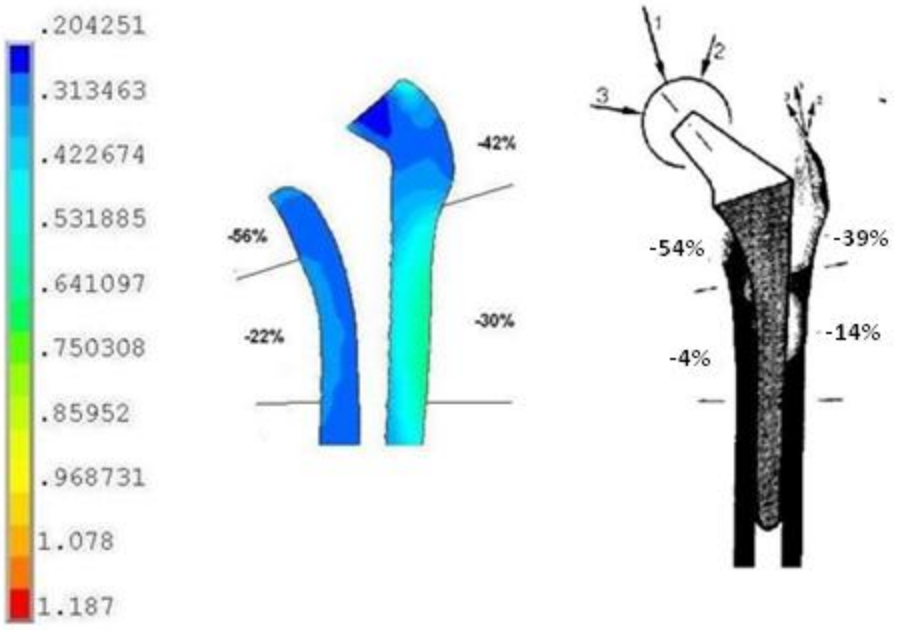

Figure 4.4: Bone Density Distribution (*g/cm*^{3}) around Titanium Implant Present Analysis (Left), Literature [75] (Right)

As can be seen in the Figure, in the greater trochanter and medial cortex bone loss with respect to the intact femur is the same in both models, whereas in the lower zones the bone loss based which is obtained from the present analysis is lower in comparison with the literature which is most likely due to the differences in the two geometries specially the longer length of the implant in the present analysis which causes the density to decrease distally and the fact that in the finite element model in this work is three dimensional unlike the two dimensional model of the literature.

4.3 A Comparison between the Thermodynamic Model and the Strain Energy Model

In this section, the thermodynamic model is compared with the classical adaptive bone remodeling model base on the strain energy density which was developed by Weinanse et al. [14]. Table 4.1 lists values of the parameters used in the strain energy based model. The initial density of the bone was set equal to the average value of the cortical and cancellous bones that is, $\rho_0=(0.32+1.64)/2=0.98$ g/cm^3. To ensure stability of the iterative process described in chapter 1, the time step was to $\Delta t=20$ time unit. Figure 4.5 shows the bone density distribution for the two models. By comparing the bone density distributions in both models, the architecture of the

femoral bone was in general comparable. The development of cancellous and cortical bone is evident in both models. The main difference is found to be between the ranges of density in the two models. This may be due to the values imposed on the lower and upper bounds of the density in the strain energy based model which in here are 0.01 and 1.74 g/cm^3, respectively. Whereas in the thermodynamic model, these values depend on the initial bone concentration, chemical rates, etc. This difference may also be attributed to the fact that in the strain energy based model, the stimulus which causes bone remodeling is the strain energy density, but in the thermodynamic model it is the coupling between chemical reactions and strain rate.

$\beta = 1\,(g/cm^3)^2/(MPa.time\ unit)$	$K = 0.004\ Jouls/g$	$E = 10500\rho^{2.57}\ (MPa)$
$s = 0.35$	$\rho_{min} = 0.01\ (g/cm^3)$	$\rho_{max} = 1.74\ (g/cm^3)$

Table 4.1: Values of Parameters in the Strain Energy Based model [9]

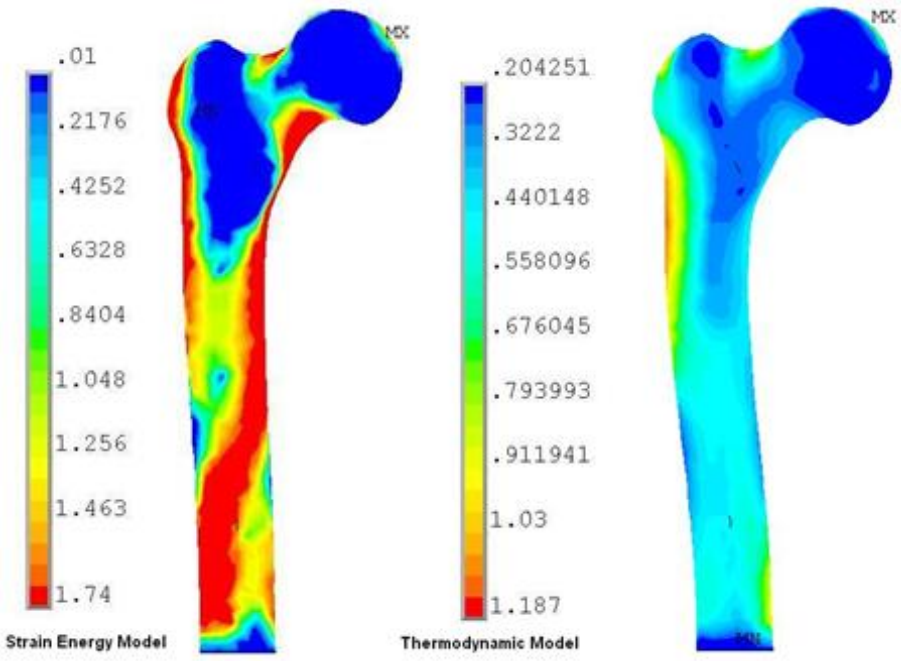

Figure 4.5: Intact Femur Density Distribution (*g/cm*^{3}) Strain Energy Model (Left), Thermodynamic Model (Right)

4.4 Titanium versus Composite Hip Stem

Since the shape of the conventional titanium implant is the same as that of the composite hip stem, it will be interesting to draw a comparison between the density distributions of the femoral bone around these two types of implants. Figure 4.6 shows the density distribution for these two implants. It is obvious that the density distribution in case of the composite implant is more ideal compared to the titanium implant. In order to examine the distribution more closely, the femur is divided into seven separate zones known as Gruen zones. In Gruen zones 7, 6 and 5, bone density distributions are almost similar in the two implants. However, in zone one, at the greater trochanter as well as zone 2, there is a considerably larger area of dense bone around the composite implant compared to the conventional titanium implant. Moving further down to the distal part of the bone, it can be seen that the bone becomes denser around the titanium implant in zones 3, 5 and the upper part of zone 4. In order to see the distribution within the femoral thickness two cross sections one proximal and one distal have been shown in Figure 4.7. The same trend is observed in here as well. The bone around the titanium implant is more resorbed in the proximal area and denser in the distal part whereas the converse holds true for the composite implant. As previously mentioned the composite implant was designed to mimic the real bone by having a composite shell with a modulus of elasticity close to the cortical bone, which encompasses a polymeric core with a modulus close to that of the cancellous bone. This can explain the extent of stress shielding reduction in this implant compared to titanium. What might be observed as a defect in both models is the extent of resorption in zones 7 and 6. However, this comparison can highlight the advantage of the composite hip stem over the titanium one.

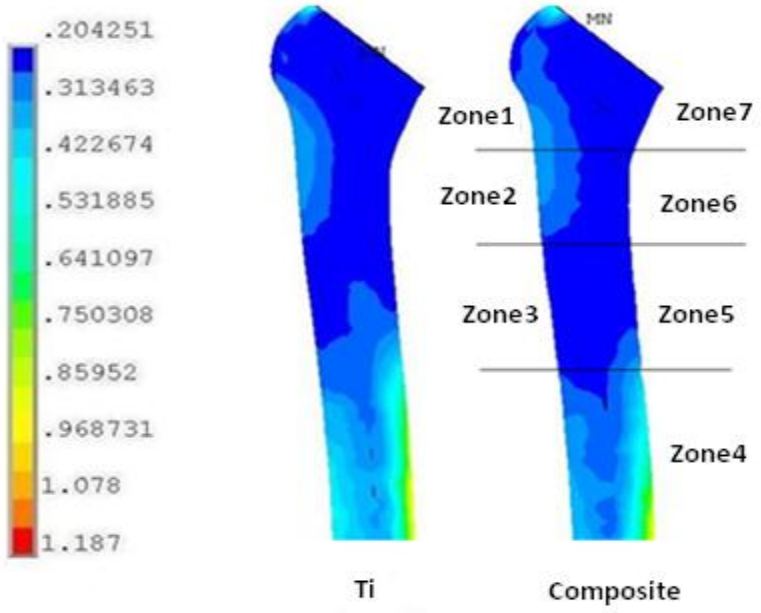

Figure 4.6: Density Distribution (g/cm^3) around Titanium and the Composite Implants

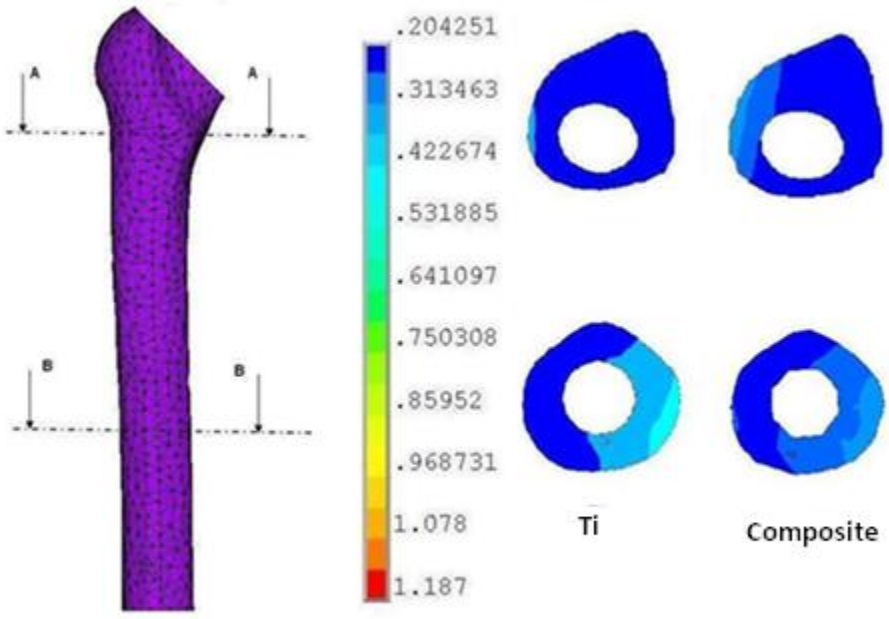

Figure 4.7: Section View of Density Distribution (g/cm^3) around Titanium and the Composite Implants

4.5 Effects of Hip Stem Geometry

Figure 4.8 shows the three dimensional view of the bone density distribution for three different implant geometries all of which were assigned the material properties of titanium.

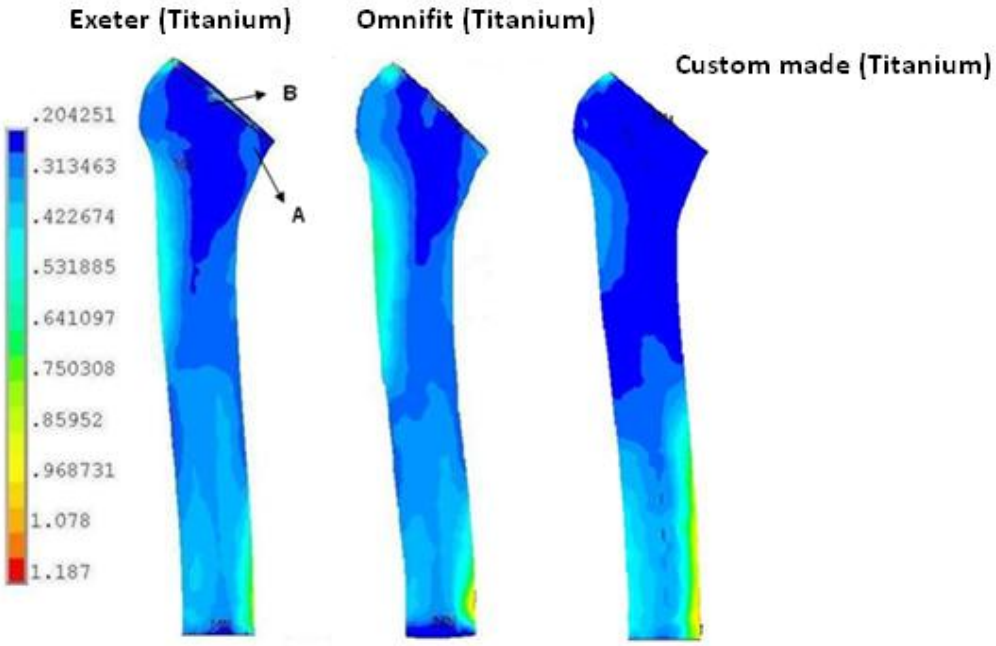

Figure 4.8: Bone Density Distribution (g/cm^3) around 3 Different Implant Geometries

Due to the extreme resorption in the medial/proximal part of the femur for the conventional titanium implant compared to the other two geometries, it seems that the conventional hip stem may not be a good choice for total hip arthroplasty compared to the other geometries. This is mainly due to the high length of this implant compared to the other two geometries which has in turn taken a bigger share of the load and has therefore resulted in more bone resorption in the proximal femur. Turning now to the Exeter and Omnifit geometries, it can be easily seen that bone loss in the proximal greater trochanter area of the bone around the Exeter implant with respect to the intact femur, is approximately 31%.Whereas, bone loss in the same area for the Omnifit geometry is around 18%. In addition, the Exeter implant shows more resorption in the areas marked as A and B in Figure 4.8. On the contrary, there is more dense bone in the distal part of the Exeter implant which makes it more susceptible to stress shielding. Based on this

comparison, the Omnifit geometry is taken as the most suitable one to study the effect of material properties in the next section.

4.6 Effects of Material Properties

In order to study the effect of material properties of the implant on bone remodeling following total hip arthroplasty, the Omnifit geometry, which was found to be the most suitable one in the previous section, is assigned different material properties. Figures 4.9 and 4.10 show the three dimensional and section views of the bone density distribution around three different implant materials, respectively. It is seen that the bone resorption in the proximal area around the CoCrMo implant is much more severe than the other two hip stems. The maximum bone loss with reference to the intact bone for the CoCrMo is found to be almost 52% in the proximal/lateral part versus approximately 30% for the composite and low modulus titanium alloy (Ti-13Nb-13Zr) hip stems in the same area. A comparison between CF/PA12 and the low modulus titanium alloy hip stems shows that not only is there a milder level of reorption in the CF/PA12 implant than the titanium one, but there is also less densification in the distal part. In particular the amount of resorption in the areas denoted by A and B is more severe in the case of the low modulus titanium alloy implant than the composite hip stem. Taking the moduli of elasticity of the implant materials into account, the above-explained comparison reflects the fact that the load transfer from the implant to the bone occurs more proximally for more flexible implants. In other words, the stress shielding phenomenon is more outstanding for the stiffer implant.

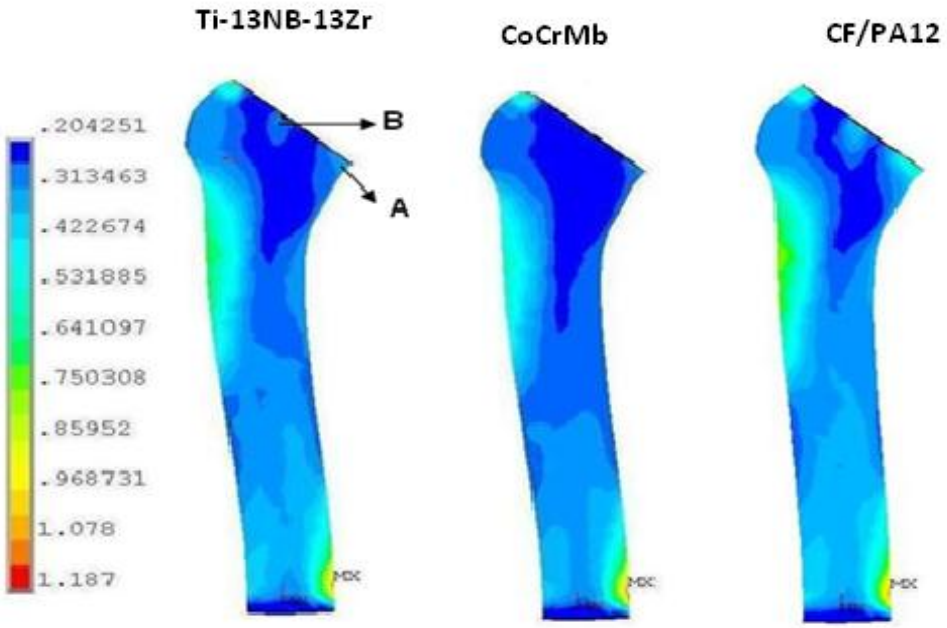

Figure 4.9: Bone Density Distribution (g/cm^3) around 3 Different Implant Materials

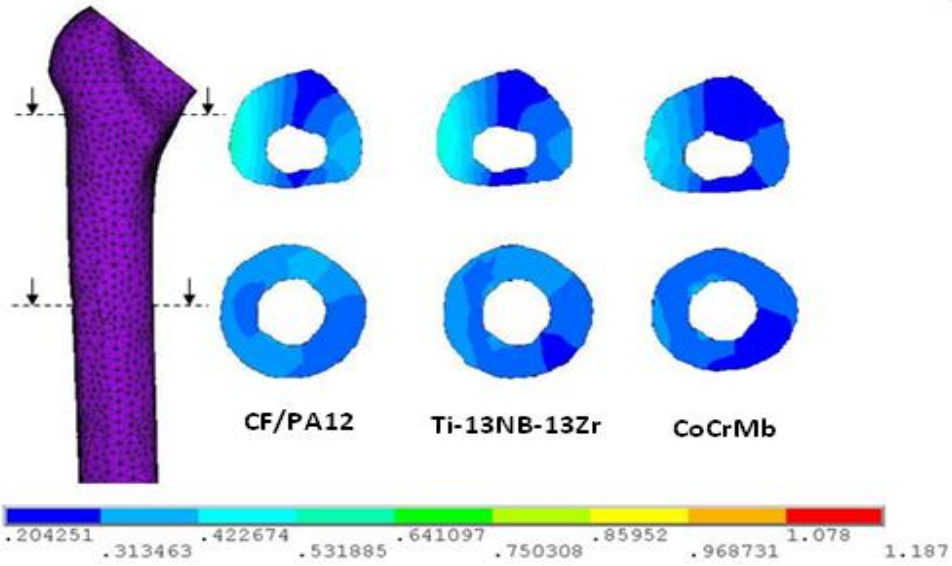

Figure 4.10: Section views of the Proximal and Distal Regions of Bone Density Distribution (g/cm^3) around 3 Different Implant Materials

4.7 Conclusions

All the results of the remodeling patterns around the hip stems based on the finite element formulation of the thermodynamic based model fit into a realistic range when compared to the literature. As previously mentioned the conventional strain energy based model takes only the mechanical stimulus into account and strongly depends on the boundary conditions imposed on the bone density as well as the size of the dead zone. However, the thermodynamic based model in the present yields more realistic results in the sense that involves the coupling between the mechanical load and the chemical reactions of the bone remodeling process.

In fact, the computer simulations confirm the clinical observation that stiffer implants result in more reorption in the proximal area and more densification in the distal part and therefore are more prone to stress shielding so that when different material properties are attributed to one particular implant geometry, the low modulus based titanium alloy (Ti-13Nb-13Zr) predicts minimal stress shielding. But it is also found that apart from the material property, the geometry is also important and the Omnifit geometry is seen to be the most suitable one among all the other geometries.

4.8 Limitations

It must be emphasized that the present model although more advanced than the models which have hitherto been reported, is still simple compared to in vivo situation. First of all, it is based on five chemical reactions including only the two stages of resorption and formation. The main limitation of this model is the difficulty to adjust the biochemical values (those expressed as constants in Table 5.1). As a matter of fact, the values of theses parameters which characterize the chemical reactions are not known and have to be obtained through experimental measurements. It has to be mentioned that the objective of this work is to study the exclusive effects of two parameters geometry and material properties of the implant by keeping other parameters as constant. So it overlooks the effects of other parameters such as the interface condition which is considered to be fully bonded in here. The present computer simulation assumed stabilized end conditions, whereas in clinical studies, the extent to which the remodeling patterns can be regarded as having reached equilibrium is usually uncertain [76]. In the present analysis it is assumed that loads are equal before and after total hip arthroplasty, whereas in reality this is not the case, In addition, the finite element model represents one

particular configuration for total hip arthroplasty and many model parameters which in reality vary with patients are regarded as constants. Therefore the results presented here are to be viewed as trends and conclusions reached are mainly qualitative rather than quantitative. Nevertheless, this simplified model is the first step in the development of a new model for the bone remodeling process based on nonequilbrium thermodynamics.

4.9 Suggestions for Future Work

The thermodynamic based model described above is based on five chemical reactions including only the two stages of resorption and formation. An ideal model should include the reactions defining bone growth control which leads to the decrease of osteoclasts concentration and therefore the decrease of the rate of bone loss. In addition, experimental facilities such as a bioreactor are needed in order to obtain values for the biochemical parameters of the model. Through the application of this model into the simulation of bone remodeling using different implants, Omnifit geometry with composite properties was found to be the most suitable choice because of minimal bone resorption in the proximal area. This calls for further probe into the possibility of designing an implant with the geometry of Omnifit which consists of a composite layer made of CF/PA12 to mimic the cortical bone and an internal polymeric core to mimic the cancellous bone which may lead to even further decrease in the detrimental phenomenon of stress shielding.

References

[1] Siopack J S , Jergesen H E ."Total Hip Arthroplasty". Western Journal of Medicine 1995; 162(3): 243–249.

[2] Figure 1.1 obtained from <http://www.osprey.medicalmultimediagroup.com/images/hip/hip_arthroplasty>

[3] Roberson J R. "Proximal Femoral Bone Loss after Total Hip Arthroplasty". Orthopedic Clinic of North America 1992; 23(2): 291-302.

[4] Sumner DR, Turner TM, Igloria R,Urban RM, Galante JO. "Functional Adaptation and Ingrowth of Bone Vary as a Function of Hip Implant Stiffness". Journal of Biomechanics 1998; 31(10): 909-17.

[5] Figure 1.2 obtained from <http://www.bananarepublican.info/Stress_shielding.htm>

[6] Gamradt SC, Lieberman JR. "Bone Graft for Revision Hip Arthroplasty: Biology and Future Applications". Clinical Orthopedics and Related Research 2003; (417):183-94.

[7] Berry D, Harmsen WS, Cabanela ME, Morrey BF. "Twenty-five-Year Survivorship of Two Thousand Consecutive Primary Charnley Total Hip Replacements". The Journal of Bone and Joint Surgery (American) 2002; 84:171-177.

[8]Kurtz S, Ong K, Lau E, Mowat F, Halpern M."Projections of Primary and Revision Hip and Knee Arthroplasty in the United States from 2005 to 2030".The Journal of Bone and Joint Surgery (American) 2007; 89:780-785.

[9] Bougherara H, Bureau M, Yahia L. "Bone Remodeling in a New Biomemtic Polymer-Composite Hip Stem". Journal of Biomedical Materials Research Part A 2010; 92(1):164-74.

[10] Frankel V, Nordin M. "Basic Biomechanics of the Skeletal System". Kimpton Publishers 1980.

[11] Ruimerman R. "Modeling and Remodeling in Bone Tissue". Technische Universiteit. Eindhoven, 2005.

[12] Deuel CR. "Development of an Adaptive 3D Model of the Human Femur to Simulate Bone Remodeling Following Hip Resurfacing and Total Hip Arthroplasties". PhD Thesis, University of California Davis, 2007.

[13] Figure 1.5 obtained from <http://www.lilly.com/pdf/bone_remodeling_process_1003.pdf>

[14] Weinans H, Huiskes R, Grootenboer HJ. "The Behavior of Adaptive Bone Remodeling Simulation Models". Journal of Biomechanics 1992; 25:1425-1441.

[15] Huiskes R, Weinans H, Grootenboer HJ,Dalstra M,Fudala B, Sloof TJ. "Adaptive Bone Remodeling Theory Applied to Prosthetic Design Analysis". Journal of Biomechanics 1987; 20:1135-1150.

[16] Levenston ME, Carter DR. " An Energy Dissipation-Based Model for Damage Stimulated Bone Adaptation". Journal of Biomechanics 1998; 31:579-586.

[17] Jee W.S.S. "Principles in Bone Physiology ". Journal of Musculoskeletal and Neuronal Interactions 2000; 1:11-13.

[18] Huiskes R, Ruimerman R, Van Lenthe GH, Janssen JD." Effects of Mechanical Forces on Maintenance and Adaptation of Form in Trabecular Bone". Nature 2000; 405:704-706.

[19] Hernandez CJ, Beaupre GS, Carter DR. "A Model of Mechano-biologic and Metabolic Influences Bone Adaptation". Journal of Rehabilitation Research and Development 2000; 37:235-244.

[20] Huiskes R, Ruimerman R, Van Lenthe GH, Janssen JD."A Computer Simulation Model Relating Bone Cell Metabolism to Mechanical Adaptation of Trabecular Bone". Computer Methods in Biomechanics and Biomedical Engineering 2001; 4: 433-448.

[21] Bougherara H, Klica V, Marsik Frantisek, Marik IA, Yahia LH. "New Predictive Model for Monitoring Bone Remodeling". Journal of Biomedical Materials Research Part A. Published Online 10 June 2010.

[22] Kroll MH." Parathyroid Hormone Temporal Effects on Bone Formation and Resorption".Bulletin of Mathematical Biology 2000; 62:163-188.

[23] Rattanakul C, Lenbury Y, Krishnamara N,Wollkind DJ. "Modeling of Bone Formation and Resorption Mediated by Parathyroid Hormone: Response to Estrogen/PTH Therapy". Biosystems 2003; 70:55-72.

[24] Komarova SV, Smith RJ, Dixon SJ, Sims SM, Wahl LM." Mathematical Model Predicts a Critical Role for Osteoclast Autocrine Regulation in the control of Bone Remodeling". Bone 2003; 33:206-215.

[25] Lemaire V, Tobin FL, Greller LD, Cho CR, Suva LJ, "Modeling the Interactions between Osteoblast and Osteoclast Activities in Bone Remodeling". Journal of Theoretical Biology 2004; 229: 293-309.

[26] Figure 1.8 obtained from <http://www.theorthopediccenter.net/services/hips.html>

[27] Bowlin GL, Wnek G. "Encyclopedia of Biomaterials and Biomedical Engineering". Informa Healthcare USA Inc 2007.

[28] Seedhom BB, Wallbridge NC."Walking Activities and Wear of Prostheses". Annals of Rheumatic Disease 1985; 44:838-843.

[29] Thompson DM. "Introduction to the Study of Human Walking: Basics of Gait Terminology" .Lectures on the Control of Human Movement of Biostatics and Epidemiology

[30] Gomez P, and J Morcuende. "Early Attempts at Hip Arthroplasty 1700s to 1900s". The Iowa Orthopedic Journal 2005; (25): 25-29.

[31] Pospula W. "Total Hip Replacement: Past, Present and Future". Kuwait Medical Journal 2004; (36):250-255.

[32] Lohmander LS, Engesaeter LB, Herberts P, Ingvarsson T, Lucht U, Puolakka TJ. "Standardized incidence rates of total hip replacement for primary hip osteoarthritis in the 5 Nordic countries: similarities and differences". Acta Orthopedica 2006; 77(5):733-40.

[33] Figure 1.13 obtained from <http://www.sheinkopmd.com/2009_08_01_archive.html>

[34] Figure 1.14 obtained from

<http://adam.about.com/encyclopedia/infectiousdiseases/Rheumatoid-arthritis.htm>

[35] Figure 1.15 obtained from < http://www.eorthopod.com/content/avascular-necrosis-hip>

[36] Figure 1.16 obtained from <http://www.rush.edu/rumc/page-1098987368010.html>

[37] Figure 1.17 obtained from
<http://osprey.medicalmultimediagroup.com/images/hip/hip_arthroplasty/>

[38] Canadian Institute for Health Information (CIHI). "Canadian Joint Replacement Registry (CJRR) 2008-2009 Annual Report: Hip and Knee Replacements in Canada". CIHI and Canadian Orthopedic Association, Ottawa, ON.

[39] Shanbhag A, Rubash HE. Jacobs JJ. "Joint Replacement and Bone Resorption: Pathology, Biomaterials and Clinical Practice". Informa Healthcare 2005.

[40] Goldberg JR, Gilbert JL, Jacobs JJ, Bauer TW, Paprosky W, Leurgans S."A Multicenter Retrieval Study of the Taper Interfaces of Modular Hip Prostheses". Clinical Orthopedics and Related Research 2002; 401:149-161.

[41] Wan Z, Dorr LD, Woodsome T, Ranawat A, Song M."Effect of Stem Stiffness and Bone Stiffness on Bone Remodeling in Cemented Total Hip Replacement". Journal of Arthroplasty 1999; 2:149-158.

[42] Woolson ST, Milbauer JP, Yue S, Maloney WJ."Fatigue Fracture of a Forged Cobalt-Chromium-Molybdenum Femoral Component Inserted with Cement. A Report of Ten Cases". The Journal of Bone and Joint Surgery 1997; 79: 1842-8.

[43] Black J. "Biological Performance of Tantalum". Clinical Materials 1994; 16:167-173.

[44] Wright TM, Goodman SP. "Implant Wear in Total Joint Replacement: Clinical and Biologic Issues, Material and Design Considerations". Rosemont: American Academy of Orthopedic Surgeons 2001.

[45] Bobyn JD, Glassman AH, Goto H, Krygier JJ, Miller JE, Brooks CE. "The Effect of Stem Stiffness on Femoral Bone Resorption after Canine Porous-Coated Total Hip Arthroplasty". Clinical Orthopedics and Related Research 1990; 261:196-213.

[46] Nicolis G, Prigoginee I." Self-Organization in Nonequilibrium Systems". John Wiley and Sons 1977.

[47]Mahenra RA. "Nonequilibrium Thermodynamics: Irreversible Thermodynamics of Physico-Chemical and Biological Processes". Dattsons 2005.

[48] De Groot SR, Mazur P. "Non-Equilibrium Thermodynamics". Dover Publications 1984.

[49] Bokstein BS, Mendelev MI, Srolovitz DJ. "Thermodynamics and kinetics in Materials Science: a Short Course". Oxford University Press 2005.

[50] Fung YC. "Biomechanics: Motion, Flow, Stress, and Growth". Springer 1990.

[51] Sears FW, Salinger GL."Thermodynamics, Kinetic Theory and Statistical Thermodynamics". Addison Wesley Publishing Company 1975.

[52] Keii T. "Heterogeneous Kinetics: Theory of Ziegler-Natta-Kaminsky Polymerization ". Springer 2004.

[53] Klika V, Marsik F. "Coupling Effect between Mechanical Loading and Chemical Reactions".

Journal of Physical Chemistry B. 2009; 113: 14689–14697.

[54] Chen ER. "Quantities, units and symbols in physical chemistry". The Royal Society of Chemistry 2007.

[55] Carter DR, Orr TE, Fyhrie DP."Relationships between Loading History and Femoral Cancellous Bone Architecture". Journal of Biomechanics 1989; 22: 231-244.

[56] Rubin C, Lanyon L. "Regulation of Bone Mass by Mechanical Strain Magnitude". Calcified Tissue International 1985; 37:411-417.

[57] Mahboob Z. "A Validated Finite Element Study of Stress Shielding in a Novel Hybrid Knee Implant". M.A.SC. Thesis, Ryerson University, Toronto, ON, Canada, 2009.

[58] Huiskes R, Chao EY."A survey of Finite Element Analysis in Orthopedic Biomechanics: the First Decade". Journal of Biomechanics 1983; 16(6): 385-409.

[59] Andriacchi TP, Galante JO, Belytschko TB, Hampton S. "A Stress Analysis of the Femoral Stem in Total Hip Prostheses". Journal of Bone and Joint Surgery 1987; 58(5) 616-624.

[60] Kwak BM, Lim OK, Kim YY, Rim K."An Investigation of the Effect of Cement Thickness on an Implant by Finite Element Stress Analysis". International Orthopedics 1978; 2(4): 315-319.

[61] Yettram AL, Wright KWJ. "Dependence of Stem Stress in Total Hip Replacement on Prosthesis and Cement Stiffness". Journal of Biomedical engineering 1980; 2:54-59.

[62] Cook SD, Klawitter JJ, Weinstein AM. "The Influence of Design Parameters on Calcar Stresses Following Femoral Head Arthroplasty". Journal of Biomedical Material Research 1980; 14(2):68-78.

[63] Sih GC, Matic P, Berman AT. "Failure Prediction of the Total Hip Prosthesis System". Journal of Biomechanics 1981; 14:833-841.

[64] Skinner HB, Cook SD, Weinstein AM, Haddad RJ. "Stress Changes in Bone Secondary to the Use of a Femoral Canal Plug with Cemented Hip Replacement". Clinical Orthopedics & Related Research 1980; 166:277-283.

[65] Huiskes R, Elangovan PT, Banens JPA, Slooff TJ. “Finite Element Computer Methods for Design and Fixation Problems of Orthopedic Implants". Biomechanics 6-B: 6th International Congress of Biomechanics 1977; 2:229-238.

[66]Valliappan S, Kjellerg S, Svensson NL."Finite Element Analysis of Total Hip Prosthesis". International Conference Proceedings on Finite Elements in Biomechanics 1980; 528-548.

[67] Ebinger T."Multiscale Modeling of Bone Remodeling". M.A.SC. Thesis, Saarland University, Germany, 2009.

[68] ANSYS Release 11.0 Documentation for ANSYS.

[69] Bougherara H, Zdero R, Shah S, Miric M, Papini M, Zalzal P, Schemitsch EH. "A Biomechanical Assessment of Modular and Monoblock Revision Hip Implants Using FE Analysis and Strain Gage Measurements". Journal of Orthopedic Surgury and Research 2010; 5-34.

[69] Bougherara H, Zdero R, Miric M, Shah S, Hardisty M, Zalzal P, Schemitsch EH. "The Biomechanics of the T2 Femoral Nailing System: A Comparison of Synthetic Femurs with Finite Element Analysis". Proceedings of the Institution of Mechanical Engineers, Part H: Journal of Engineering in Medicine 2009; 223(3):303-314.

[70] Bougherara H, Zdero R, Mahboob Z, Dubov A, Shah S, Schemitsch EH. "The Biomechanics of a Validated Finite Element Study of Stress Shielding in a Novel Hybrid Total Knee Replacement". Proceedings of the Institution of Mechanical Engineers, Part H: Journal of Engineering in Medicine (In Press).

[71] Kuhl E, Balle E, "Computational Modeling of Hip Replacement Surgery: Total Hip Replacement vs. Hip Resurfacing". Technische Mechanik 2005; 107-114.

[72] Anonymous Stryker Corporation, Mahwah, NJ, USA. Obtained from <http://www.Stryker.Com>.

[73] Truenge LH, Kuliwaba J, Tsangari H, Fazzalari N. "Differential Gene Expression of Bone Anabolic Factors and Trabecular Bone Architectural Changes in the Proximal Femoral Shaft of Primary Hip Osteoarthritis Patients ".Arthritis Research and Therapy 2006; 8:R188.

[74] Weinans H, Huiskes R, Grootenboer HJ. "Effects of material Properties of Femoral hip Components on Bone Remodeling". Journal of Orthopedic research 1992; 10:845-853.

[75] Huiskes R Weinans H, Rietbergen B. "The Relationship between Stress Shielding and Bone Resorption Around Total Hip Stems and the Effects of Flexible Materials". Clinical Orthopedics and Related Research 1992; 274:124-134.